Available online at www.sciencedirect.com
ScienceDirect
Journal of Computational Physics 227 (2008) 9241–9270
JOURNAL OF COMPUTATIONAL PHYSICS
www.elsevier.com/locate/jcp

A conservative approximation to compressible two-phase flow models in the stiff mechanical relaxation limit

Vincent Deledicque, Miltiadis V. Papalexandris *

Département de Mécanique, Université catholique de Louvain, 1348 Louvain-la-Neuve, Belgium

Received 18 May 2007; received in revised form 7 December 2007; accepted 11 December 2007
Available online 23 December 2007

Dedicated to Professor Anthony Leonard

Abstract

In this article, we present and analyze a conservative approximation to reduced one-pressure one-velocity models for compressible two-phase flows that contain non-conservative products. This approximation is valid when certain material properties of the two phases are considerably different from each other. Although it cannot be applied to arbitrary mixtures, it is applicable to many heterogeneous mixtures of technological interest. Herein, we derive the Rankine–Hugoniot relations and Riemann invariants for the homogeneous part of the proposed model and develop an exact Riemann solver for it. Further, we investigate the structure of the steady two-phase detonation waves, with inert or reactive solid particles, admitted by the proposed model. Comparisons with the corresponding gaseous detonations are also made. Moreover, we derive a lower limit for the propagation speed of steady two-phase detonations in the case of reactive particles. At the limiting case of very dilute mixtures, this minimum speed tends to the Chapman–Jouguet velocity of gaseous detonations. Finally, we report on numerical simulations of the transmission of a purely gaseous detonation to heterogeneous mixtures containing inert or reactive solid particles. The effect of the solid particles on the structure of the resulting two-phase detonation is discussed in detail.

Keywords: Compressible two-phase flows; Reduced models; Heterogeneous detonation; Hyperbolic conservative laws

1. Introduction

Compressible two-phase flows arise in various natural and technological applications such as sandstorms, volcanic eruptions, power plants, chemical plants, solid rocket motors, detonation coatings, deflagration-to-detonation transition in granular explosives, and others. These flows are quite difficult to study due to the presence of complex physical processes (chemical reactions and/or phase transitions, momentum and energy exchange between the phases, etc.) and due to the large number of spatial and temporal scales associated with

* Corresponding author. Tel.: +32 (0) 10 47 88 83; fax: +32 (0) 10 45 26 92.
E-mail address: miltos@uclouvain.be (M.V. Papalexandris).

0021-9991/$ - see front matter © 2008 Elsevier Inc. All rights reserved.
doi:10.1016/j.jcp.2007.12.011

those processes. In this article, we propose a conservative approximation to models for compressible two-phase flows in the limit of stiff mechanical relaxation. Subsequently, we solve the resulting system of equations numerically and perform simulations of detonations carrying small amounts of solid particles.

Over the years various approaches have been proposed to develop mathematical models for compressible two-phase flows. In general, such models are obtained by either an averaging approach or a mixture-theory approach. Averaging approaches are based on kinetic theories and consider one phase as an ensemble of interacting particles embedded in a carrier fluid medium. The number density of particles expressed in an appropriate phase space (coordinate-velocity space for instance) is the distribution function and obeys a Boltzmann-type equation. This equation is integrated over the phase-space to derive the governing equations for the medium, see Drew and Passman [1] and Enwald et al. [2]. This procedure, referred to as ensemble averaging, can be replaced by time or volume averaging, provided that the ergodic hypothesis is satisfied. However, the complexity of interactions between the solid particles (anelastic collisions, different particle sizes, three-body collisions etc.) and the presence of a surrounding fluid medium does not allow a straightforward application of kinetic theories. As a result, kinetic-theory approaches have not yet resulted in the development of a sufficiently sophisticated model, i.e., a model that is able to describe all the subtleties of the flow-fields of interest.

On the other hand, mixture approaches treat the phases as two separate but coexisting continua that are in thermodynamic non-equilibrium with each other. The balance equations can be derived by variational principles or by application of irreversible thermodynamics theories, or even by heuristic approaches. A well-known model in this category has been proposed by Baer and Nunziato [3], who aimed at describing a granular explosive in which the gaseous phase fills completely the interstitial pores. In this model, each phase is assigned a set of thermodynamic variables and a velocity. The source terms describing interactions between the two phases are derived by employing the entropy inequality for the mixture. Further, an evolutionary equation for the porosity of the mixture is obtained. According to this, the volume fraction of the solid phase is advected with the solid velocity. However, this automatically implies that, for a saturated medium, the gaseous volume fraction is also advected with the solid velocity, thus introducing an important asymmetry to the mathematical model. An important characteristic of this model is that, due to the momentum exchange between the two phases, the momentum and energy equations of each phase contain non-conservative products, i.e., terms which cannot be written in divergence form. These terms are often referred to as ‘‘nozzling terms”, due to their analogy to similar terms that appear in the Euler equations for 1D duct flow.

This model, although quite popular, is not free of deficiencies, as pointed out by Bdzil et al. [4]. For example, the model does not treat in a thermodynamically consistent way the volume-fraction dependence of the solid phase free energy, see also Powers et al. [5]. Moreover, the source terms proposed in [3] are only one realization of the many possibilities that are compatible with the dissipation inequality as employed in [3]. The authors in [4] took advantage of this flexibility to suggest improvements in the construction of the exchange terms. The homogeneous part of the original model remained however unchanged. In particular, non-conservative terms were still present.

Also, Saurel and Abgrall [6] proposed a new compressible two-phase model by applying volume averaging and by neglecting all dissipative terms everywhere except at the interfaces. Their formulation provides some flexibility in the choice of interfacial pressure and velocity. Motivated by heuristic arguments, Saurel and Abgrall [6] estimated the interfacial pressure as being the mixture pressure, and the interfacial velocity as being the weighted average of the phase velocities.

More recently, Papalexandris [7] applied the classical theory of irreversible processes to derive a model for saturated heat-conducting and viscous mixtures of a granular medium and a fluid. This theory provided a straightforward way to properly take into account all thermodynamic forces that appear in the balance equations of the mixture. Therefore, new constitutive relations for the phase interactions were obtained, as well as for the (non-Newtonian) viscosity of the granular medium. Nonetheless, in the hyperbolic limit (no dissipation mechanism inside each phase) the homogeneous part of the system was very similar to the earlier models [3,4]. In particular, both volume fractions are advected with the velocity of the solid phase, and non-conservative products appear in the momentum and energy equations of both phases.

As can be observed, most two-phase models do contain non-conservative products. Some modeling and numerical studies ignore these terms, either by choice, Gonthier and Powers [8], or by convenience,

Papalexandris [9,10], but this can potentially lead to violation of the entropy inequality. Therefore, it is generally accepted that the flow models should include these terms. Unfortunately, their presence introduces serious analytical and computational difficulties. First of all, weak solutions of the equations cannot be defined in the standard sense of distributions. As a result, the Rankine–Hugoniot relations for a shock cannot be defined in an unambiguous way. More important, non-conservative products are responsible for the ill-possedness of the associated homogeneous Riemann problem, Andrianov and Warnecke [11], Deledicque and Papalexandris [12], Powers [13] and Vreman [14]. In particular, there are initial conditions for which the Riemann problem might possess two solutions or no solution at all. According to the authors in [12], this is indicative of a breakdown of the validity of the afore-mentioned hyperbolic flow models.

On the other hand, some authors adopted the point of view that it is not necessary to resolve all scales of the flow with the same level of accuracy. For example, in certain applications, estimates reveal that the length scales for mechanical equilibration are very small in comparison with the ones associated with thermal or chemical equilibration, see Kapila et al. [15]. This implies that, for global flow structures, carrying two velocity or two-pressure variables could be a superfluous complexity. Thus, it would be meaningful to reduce the complete two-phase models to simplified one-pressure one-velocity models. Such a reduced model has been proposed in [15] for instance. According to it, the thin layers across which all dissipative effects due to velocity and pressure non-equilibrium take place, are modeled as exact discontinuities (shocks). This is equivalent to assuming an infinitely fast relaxation procedure for mechanical equilibrium. It has been shown that this model is thermodynamically consistent, in the sense that it does not violate the entropy inequality.

However, this model still contains non-conservative products and therefore, Rankine–Hugoniot relations cannot be defined in an unambiguous manner. In particular, an additional closure relation is needed to provide a full set of jump conditions. This relation may be provided by some regularization procedure. Such a regularization has been proposed in [15], and more recently, by Saurel et al. [16]. The latter takes into account the finite thickness of shock waves, thus enabling the derivation of a kinematic relation that can serve as an additional jump condition. Their approach, although not free of certain restrictions, can produce shock pressures and velocities that compare well with experimental results. Unfortunately, even with this additional relation, the well-possedness of the Riemann problem is not guaranteed. This has a profound effect in the design of algorithms for the numerical treatment of the governing equations because most modern schemes for compressible flow simulations are based on a Riemann solver.

In this article, we propose a way to circumvent these difficulties by employing an additional assumption, besides the infinitely fast relaxation. Under the hypothesis that the solid phase density and sound speed are much larger than the gaseous phase density and sound speed, respectively, we demonstrate that these reduced models can in fact be written in conservative form. This hypothesis is realistic for many heterogeneous mixtures. The evolutionary equation for the volume fraction then simply expresses conservation of the solid volume, apart from volume exchanges due to heat transfer effects and combustion of the solid particles.

This paper is organized as follows. In Section 2 we present the one-pressure one-velocity model developed in [15] and derive the proposed conservative approximation to it. Although this two-phase model can be applied to various compressible flow applications, we focus our attention to the study of detonations in gases carrying solid particles. Hence, we augment the system of conservation equations by conservation laws for the particle number density and gaseous reactant mass fraction. The entire system can be cast in divergence (conservative) form. In Section 3 we perform the characteristic analysis of the reduced conservative model, and derive the Riemann invariants and Rankine–Hugoniot shock relations. Subsequently, we briefly describe the numerical procedure employed to solve the Riemann problem associated with the system in hand. In Section 4, we present a steady wave analysis for the governing set of equations. The structures of these waves are compared with the ones of the corresponding gaseous detonations (ZND waves). We also establish, for particular cases, a minimum propagation speed of these steady waves, equivalent to the CJ speed of gaseous detonations. Finally, in Section 5, we consider the transmission of a gaseous detonation to a heterogeneous mixture, containing reacting or inert solid particles, and discuss the results obtained by 1D numerical simulations. We also provide the results of a preliminary 2D simulation.

2. Presentation of the mathematical model

In this study, we consider solid particles dispersed in a gaseous medium. The flow of this mixture is assumed to be inviscid and non-heat-conducting, in other words we are interested in flows where compressibility effects are dominant. Both phases are modeled as two separate but coexisting continua. Each phase is assigned a volume fraction ϕ_α and a density ρ_α, where $\alpha = \mathrm{s}, \mathrm{g}$ and "s" and "g" denote the solid and gaseous phase, respectively. It is assumed that the mixture is saturated, i.e., that $\phi_\mathrm{s} + \phi_\mathrm{g} = 1$. Under the hypothesis of stiff mechanical relaxation, the pressures and velocities of each phase are identical, henceforth denoted by p and u. Experimental evidence for the validity of this assumption has been discussed in [15], in the context of deflagration-to-detonation transition in granular materials.

The gaseous phase consists of the reactive species A and the inert species B. These two substances are assumed to have equal specific heats. The species A reacts according to

$$A \rightarrow B. \tag{1}$$

Let z denote the gaseous reactant mass fraction. It satisfies $0 < z < 1$ and it equals unity when the gaseous phase consists purely of A and zero when the gaseous phase consists only of the inert substance B.

The solid phase consists of a single substance, C, which can react according to

$$C \rightarrow B. \tag{2}$$

For convenience, it is assumed that the particle diameter d_s is identical for all particles. The solid volume fraction is related to the particle number density N_s via

$$\phi_\mathrm{s} = N_\mathrm{s} \frac{\pi d_\mathrm{s}^3}{6}. \tag{3}$$

The mixture density ρ and the mixture specific total energy e_t are given by

$$\rho = \phi_\mathrm{g}\rho_\mathrm{g} + \phi_\mathrm{s}\rho_\mathrm{s}, \tag{4}$$

$$\rho e_\mathrm{t} = \phi_\mathrm{g}\rho_\mathrm{g}e_\mathrm{g} + \phi_\mathrm{s}\rho_\mathrm{s}e_\mathrm{s} + \rho\frac{u^2}{2} + q_\mathrm{g}\phi_\mathrm{g}\rho_\mathrm{g}z + q_\mathrm{s}\phi_\mathrm{s}\rho_\mathrm{s}, \tag{5}$$

where e_g and e_s denote the gaseous and solid specific internal energies, respectively, q_g is the heat release from the gaseous reaction (1), and q_s is the heat release from the heterogeneous reaction (2).

The governing equations of the heterogeneous mixture are

$$\frac{\partial \phi_\mathrm{g}\rho_\mathrm{g}}{\partial t} + \frac{\partial \phi_\mathrm{g}\rho_\mathrm{g}u}{\partial x} = M, \tag{6a}$$

$$\frac{\partial \phi_\mathrm{s}\rho_\mathrm{s}}{\partial t} + \frac{\partial \phi_\mathrm{s}\rho_\mathrm{s}u}{\partial x} = -M, \tag{6b}$$

$$\frac{\partial \rho u}{\partial t} + \frac{\partial (\rho u^2 + p)}{\partial x} = 0, \tag{6c}$$

$$\frac{\partial \rho e_\mathrm{t}}{\partial t} + \frac{\partial (\rho e_\mathrm{t} u + pu)}{\partial x} = 0, \tag{6d}$$

$$\frac{\partial \phi_\mathrm{g}}{\partial t} + u\frac{\partial \phi_\mathrm{g}}{\partial x} = L\frac{\partial u}{\partial x} - S, \tag{6e}$$

$$\frac{\partial \phi_\mathrm{g}\rho_\mathrm{g}z}{\partial t} + \frac{\partial \phi_\mathrm{g}\rho_\mathrm{g}zu}{\partial x} = Q, \tag{6f}$$

$$\frac{\partial N_\mathrm{s}}{\partial t} + \frac{\partial N_\mathrm{s}u}{\partial x} = 0. \tag{6g}$$

Eqs. (6a) and (6b) are the mass balance laws for each phase with M representing the mass exchange between the two phases due to the burning of the solid particles. In this study, the following ignition-type mechanism has been considered, see Papalexandris [9],

$$M = \begin{cases} 0, & T_s < T_{ign}, \\ K_s \phi_s \rho_s / d_s^2, & T_s \geqslant T_{ign}, \end{cases} \tag{7}$$

where K_s is the time constant of the particle burning, T_s is the temperature of the particles and T_{ign} is the ignition temperature beyond which particles begin to react. Temperature gradients inside the particles are neglected.

Eqs. (6c) and (6d) are the momentum and energy conservation laws of the mixture, respectively. Further, (6e) is an evolution equation for the volume fraction, proposed in [15]. In this relation,

$$L = \frac{\rho_s c_s^2 - \rho_g c_g^2}{\frac{\rho_g c_g^2}{\phi_g} + \frac{\rho_s c_s^2}{\phi_s}}, \tag{8}$$

where c_α represents the sound speed of phase α, and S describes the volume fraction changes due to heat and mass transfer between both phases

$$S = \frac{H(T_g - T_s)\left(\frac{\Gamma_g}{\phi_g} + \frac{\Gamma_s}{\phi_s}\right) - \left(\frac{c_g^2}{\phi_g} + \frac{c_s^2}{\phi_s}\right) M}{\frac{\rho_g c_g^2}{\phi_g} + \frac{\rho_s c_s^2}{\phi_s}}. \tag{9}$$

Here T_s and T_g are the solid and gas temperatures, respectively, whereas Γ_s and Γ_g are the solid and gas Grüneisen coefficients, respectively. Further, H is the heat transfer coefficient and satisfies, [9],

$$H = \pi \frac{c_{pg} Nu}{Pr} \mu d_s N_s. \tag{10}$$

In this relation, c_{pg} is the specific heat of the gaseous phase, Nu and Pr are the Nusselt and Prandtl numbers, respectively, and μ is the gas viscosity. An empirical correlation of Knudsen and Katz [17] is employed for the calculation of Nu. However, as the two phases move at the same speed, that relation predicts a constant value, $Nu = 2$. Also, an empirical relationship, given by Chapman and Cowling [18], is employed for the calculation of the gas viscosity, as a function of T_g

$$\mu = \mu_0 \left(\frac{T_g}{T_0}\right)^{0.77}, \tag{11}$$

where μ_0 is the gas viscosity at $T_0 = 273\,\mathrm{K}$.

Further, Eq. (6f) describes the evolution of the reactant mass fraction z. In this equation, Q represents the gaseous reaction rate. Herein, Q is modeled by an one-step Arrhenius law

$$Q = -K_g \phi_g \rho_g z \exp\left(\frac{-E_a}{R T_g}\right), \tag{12}$$

where K_g is the reaction's pre-exponential factor, E_a is the activation energy and R is the gas constant. Finally, Eq. (6g) expresses the conservation of the number density of the particles. Although not employed here, phenomena such as breakup or coalescence of particles can be modeled with a suitable source term in (6g).

Eqs. (6a)–(6g) constitute a hyperbolic system, which cannot be put in conservative form because of the non-conservative product appearing in (6e). This implies that weak solutions cannot be defined in the standard sense of distributions and, therefore, Rankine–Hugoniot relations for the system in hand cannot be defined in an univocal manner, [19]. As mentioned above, to circumvent this difficulty one can employ a closure relation by considering dispersed shock profiles instead of exact ones, [16]. However, this additional relation is not the Rankine–Hugoniot of (6e) and, therefore, existence and uniqueness of the resulting Riemann problem cannot be guaranteed. This makes the design of algorithms for the numerical treatment of (6) very cumbersome since most of the modern schemes for compressible flow simulations are based on a Riemann solver.

Herein we propose an alternative way around these difficulties. In particular, we consider a conservative approximation of the system (6). Although this approximation cannot be valid for arbitrary materials, it is

still applicable to a large class of heterogeneous mixtures. In order to fix ideas, let us assume that both phases obey a stiffened gas equation of state,

$$e_\alpha = \frac{p + \gamma_\alpha P_\alpha}{(\gamma_\alpha - 1)\rho_\alpha} = \frac{p + \gamma_\alpha P_\alpha}{p + P_\alpha} c_{v,\alpha} T_\alpha, \tag{13}$$

where γ_α, P_α and $c_{v,\alpha}$ are material specific constants. The speed of sound is given by

$$\rho_\alpha c_\alpha^2 = \gamma_\alpha (p + P_\alpha). \tag{14}$$

The conservative approximation we propose is based on the hypothesis that

$$P_\mathrm{g} \ll p \ll P_\mathrm{s} \tag{15}$$

and

$$\gamma_\mathrm{g} < \gamma_\mathrm{s}. \tag{16}$$

In fact, a wide variety of flows of heterogeneous mixtures of technological interest do satisfy these inequalities. The inequalities (15) and (16) permit us to write

$$\frac{\rho_\mathrm{g} c_\mathrm{g}^2}{\rho_\mathrm{s} c_\mathrm{s}^2} \approx \frac{\gamma_\mathrm{g} p}{\gamma_\mathrm{s} P_\mathrm{s}} \ll 1. \tag{17}$$

By virtue of (17), L can be approximated as

$$L = \phi_\mathrm{s}\phi_\mathrm{g} \frac{1 - \frac{\rho_\mathrm{g} c_\mathrm{g}^2}{\rho_\mathrm{s} c_\mathrm{s}^2}}{1 - \phi_\mathrm{s}(1 - \frac{\rho_\mathrm{g} c_\mathrm{g}^2}{\rho_\mathrm{s} c_\mathrm{s}^2})} \approx \phi_\mathrm{s}. \tag{18}$$

Similarly,

$$S \approx \frac{H(T_\mathrm{g} - T_\mathrm{s})(\Gamma_\mathrm{g}\phi_\mathrm{s} + \Gamma_\mathrm{s}\phi_\mathrm{g}) - (c_\mathrm{g}^2\phi_\mathrm{s} + c_\mathrm{s}^2\phi_\mathrm{g})M}{\phi_\mathrm{g}\rho_\mathrm{s} c_\mathrm{s}^2}. \tag{19}$$

We mention that even for higher pressures, i.e., $p > P_\mathrm{s}$, this above approximation is still valid to a certain extent because, typically, $\gamma_\mathrm{s} > \gamma_\mathrm{g}$.

The advantage of this simplification is that the evolution equation for the volume fraction can be expressed in conservative form, and the system of governing equations becomes

$$\frac{\partial \phi_\mathrm{g}\rho_\mathrm{g}}{\partial t} + \frac{\partial \phi_\mathrm{g}\rho_\mathrm{g} u}{\partial x} = M, \tag{20a}$$

$$\frac{\partial \phi_\mathrm{s}\rho_\mathrm{s}}{\partial t} + \frac{\partial \phi_\mathrm{s}\rho_\mathrm{s} u}{\partial x} = -M, \tag{20b}$$

$$\frac{\partial \rho u}{\partial t} + \frac{\partial (\rho u^2 + p)}{\partial x} = 0, \tag{20c}$$

$$\frac{\partial \rho e_\mathrm{t}}{\partial t} + \frac{\partial (\rho e_\mathrm{t} u + p u)}{\partial x} = 0, \tag{20d}$$

$$\frac{\partial \phi_\mathrm{s}}{\partial t} + \frac{\partial \phi_\mathrm{s} u}{\partial x} = S, \tag{20e}$$

$$\frac{\partial \phi_\mathrm{g}\rho_\mathrm{g} z}{\partial t} + \frac{\partial \phi_\mathrm{g}\rho_\mathrm{g} z u}{\partial x} = Q, \tag{20f}$$

$$\frac{\partial N_\mathrm{s}}{\partial t} + \frac{\partial N_\mathrm{s} u}{\partial x} = 0. \tag{20g}$$

At this point it is interesting to compare the limits of this model with the one of system (6) at very dilute or very dense mixtures. In the case of a very dilute mixture, i.e., when $\phi_\mathrm{s} \to 0$, L tends to the same value for both models

$$\lim_{\phi_\mathrm{s} \to 0} L = 0, \tag{21}$$

see Eqs. (8) and (18). At this limit, the evolution equation for the volume fraction is the same for both models. On the other hand, for very dense mixtures, the models have different limits. Indeed, for the system (6) we have

$$\lim_{\phi_s \to 1} L = 0, \tag{22}$$

whereas for the approximate model (6) we have

$$\lim_{\phi_s \to 1} L = 1, \tag{23}$$

It is thus expected that at this limit the two models behave quite differently, which implies that the approximate model is no longer valid.

As mentioned earlier, the proposed simplified model is derived by complete two-pressure two-velocity models by use of two main approximations. These are (i) infinitely fast mechanical relaxation between the two phases and (ii) inequality (17). In general, these approximations, hence the model itself, are not valid in the entire range of physical parameters involved in two-phase flows. Therefore, the proposed model is applicable within a certain range of physical parameters only. Nonetheless, it is expected that its range of validity is of physical and technological interest.

In order to support the above argument, we provide a comparison between the predictions of the proposed reduced model and the complete two-pressure two-velocity model of Gonthier and Powers [8]. That model amounts to a conservative hyperbolic system of balance laws because it does not take into account non-conservative products. It is generally accepted that non-conservative products should be included in two-phase models, as done in [3,4,6,7] and elsewhere. However, our choice to use a conservative model for comparisons has been dictated by the fact that the Riemann problem of hyperbolic models for two-phase flows containing non-conservative products is ill-posed; see [12]. This, in turn, makes the development of numerical algorithms for non-conservative models very problematic. As a matter of fact, this ill-possedness has been our main motivation for deriving a reduced conservative model.

In our comparisons, we have examined the profiles of a steady two-phase detonation wave. An analysis of the steady-wave profile admitted by the proposed reduced model and a numerical procedure for solving them is given in Section 3. The equations of the complete model [8] are integrated via a first-order shock-capturing algorithm using an approximate HLL-type Riemann solver. The two-phase detonation is initiated with a moving piston. The compression of the heterogeneous mixtures results in the formation of a stable detonation wave. In our simulation we have imposed wall conditions on the left boundary and inflow conditions on the right boundary. The simulation is performed in the reference frame of the moving piston. The piston velocity is 2500 m/s. Further, the physical parameters have been set at,

$$\gamma_g = 1.333, \quad P_g = 0, \quad \gamma_s = 4.5, \quad P_s = 20 \times 10^8\,\mathrm{Pa},$$
$$c_{v,g} = 2\,\mathrm{kJ/kg\,K}, \quad c_{v,s} = 4\,\mathrm{kJ/kg\,K}, \quad q_g = 5\,\mathrm{MJ/kg},$$
$$K_g = 2 \times 10^6 s^{-1}, \quad E_{ag} = 3,5\,\mathrm{MJ/kg}, \quad \mu_c = 1\,\mathrm{kg/(ms)},$$

Finally, the solid volume fraction of the initially quiescent medium is set at $\phi_s = 10^{-5}$. With these values, the simulation with the complete model [8] predicted a detonation propagating at a speed $D = 3580\,\mathrm{m/s}$.

Figs. 1–4 show pressure, velocity, temperature and solid volume fraction profiles, respectively, as predicted by the two models. In these figures, it can be observed that the thermal relaxation zone is much longer than the pressure and velocity relaxation zones. Moreover, except for a narrow region behind the precursor shock, which is the mechanical relaxation zone, the two models predict very similar profiles. These results suggest that the proposed reduced model can in fact provide reliable predictions for a certain range of physical parameters of technological interest.

At this point we should repeat that the predictions of our proposed model are correct if condition (4.17) is satisfied. This condition is in addition to the hypothesis of stiff mechanical relaxation. In other words, (4.17) is necessary but not sufficient. In fact, there can be cases in which (4.17) is valid but the stiff mechanical relaxation hypothesis is not. These cases can arise in dilute mixtures with low shock pressures.

Also, in the example above, the thermal relaxation zone is much longer than the mechanical relaxation zone but the width of the later is at the order of the width of the reaction zone and, thus, non-negligible. Therefore,

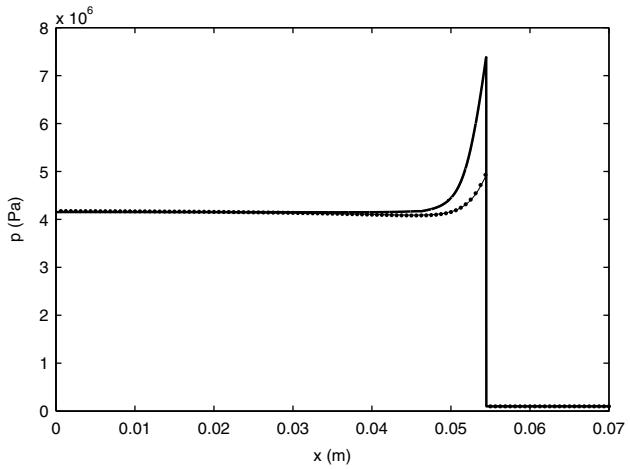

Fig. 1. Comparison between the mixture pressure profile for a steady detonation obtained by the reduced conservative model (dotted line) and the gas pressure (thin line) and solid pressure (thick line) obtained by a complete two-velocity two-pressure model. The physical parameters are given in page 10.

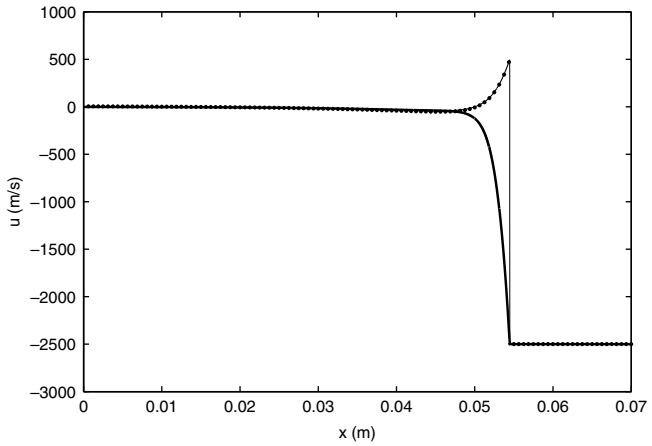

Fig. 2. Comparison between the mixture velocity profile for a steady detonation obtained by the reduced conservative model (dotted line) and the gas velocity (thin line) and solid velocity (thick line) obtained by a complete two-velocity two-pressure model. The physical parameters are given in page 10.

the reduced model cannot describe the fine structures of the flow inside the reaction zone. Instead, it may only predict the evolution of the mixture's velocity and pressure. The prediction of these average values will be correct if condition (4.17) is satisfied. This is indeed the case for the example shown above. In this particular example, the proposed reduced model tracks very well with the gas values of the complete model because the solid mass fraction is very small and, therefore, the mixture's flow variables are largely influenced by those of the gaseous phase.

3. Characteristic analysis and solution of the Riemann problem

As mentioned above, most modern numerical algorithms for compressible flows are based on a (approximate or exact) solution of the Riemann problem of the governing equations. In this section, we derive the Rankine–Hugoniot relations and the Riemann invariants that hold along the characteristic curves of the homogeneous part of the system (20). These relations are the necessary and sufficient ingredients for the design of a Riemann solver.

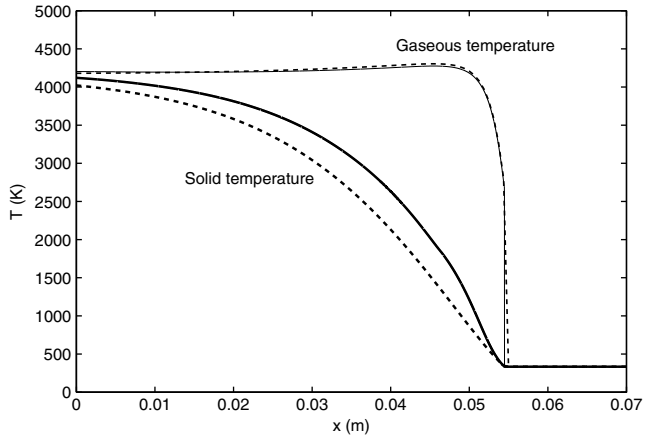

Fig. 3. Comparison between the gas temperature (thin dotted line) and the solid temperature (thick dotted line) for a steady detonation obtained by the reduced conservative model and the gas temperature (thin line) and solid temperature (thick line) obtained by a complete two-velocity two-pressure model. The physical parameters are given in page 10.

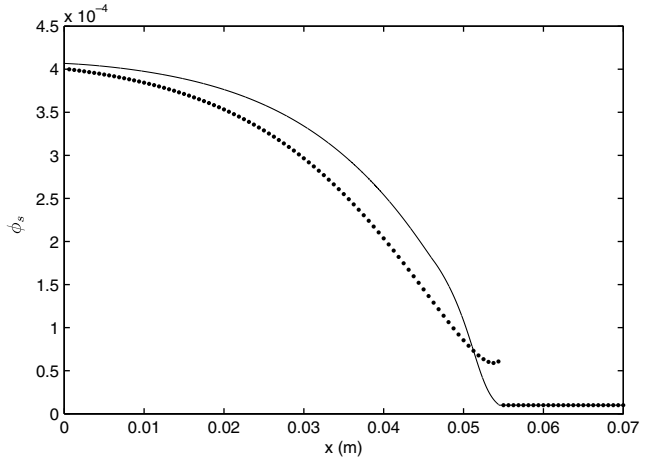

Fig. 4. Comparison between the solid volume fraction profile for a steady detonation obtained by the reduced conservative model (dotted line) and the one obtained by a complete two-velocity two-pressure model (solid line). The physical parameters are given in page 10.

3.1. Characteristic analysis

By defining $U = (\rho_g, \rho_s, u, p, \phi_s, z, N_s)$, the governing equations (20) can be written in the compact form

$$\frac{\partial U}{\partial t} + F(U)\frac{\partial U}{\partial x} = G(U) \tag{24}$$

with

$$F(U) = \begin{pmatrix} u & 0 & \rho_g/\phi_g & 0 & 0 & 0 & 0 \\ 0 & u & 0 & 0 & 0 & 0 & 0 \\ 0 & 0 & u & 1/\rho & 0 & 0 & 0 \\ 0 & 0 & \rho c^2 & u & 0 & 0 & 0 \\ 0 & 0 & \phi_s & 0 & u & 0 & 0 \\ 0 & 0 & 0 & 0 & 0 & u & 0 \\ 0 & 0 & N_s & 0 & 0 & 0 & u \end{pmatrix},$$

$$G(U) = \begin{pmatrix} (M + \rho_g S)/\phi_g \\ -(M + \rho_g S)/\phi_g \\ 0 \\ \hat{g} \\ S \\ (Q - zM)/(\phi_g \rho_g) \\ 0 \end{pmatrix},$$

where

$$\hat{g} = \frac{M(e_s - e_g + q_s) - q_g Q + (M + \rho_s S)\rho_s \frac{\partial e_s}{\partial \rho_s} - (M + \rho_g S)\rho_g \frac{\partial e_g}{\partial \rho_g}}{\phi_g \rho_g \frac{\partial e_g}{\partial p} + \phi_s \rho_s \frac{\partial e_s}{\partial p}}. \tag{25}$$

In these expressions, c is the mixture sound of speed, defined by

$$c^2 = \frac{1}{\rho}\left(\frac{p - \rho_g^2 \frac{\partial e_g}{\partial \rho_g}}{\phi_g \rho_g \frac{\partial e_g}{\partial p} + \phi_s \rho_s \frac{\partial e_s}{\partial p}}\right). \tag{26}$$

The eigenvalues of $F(U)$ are

$$\begin{aligned} &\lambda_1 = u - c, \\ &\lambda_2 = u + c, \\ &\lambda_3 = \lambda_4 = \lambda_5 = \lambda_6 = \lambda_7 = u \end{aligned} \tag{27}$$

and the corresponding right eigenvectors are

$$r_1 = \left(-\tfrac{\rho_g}{\phi_g c},\ 0,\ 1,\ -\rho c,\ -\tfrac{\phi_s}{c},\ 0,\ -\tfrac{N_s}{c}\right), \tag{28a}$$

$$r_2 = \left(\tfrac{\rho_g}{\phi_g c},\ 0,\ 1,\ \rho c,\ \tfrac{\phi_s}{c},\ 0,\ \tfrac{N_s}{c}\right), \tag{28b}$$

$$r_3 = (1,\ 0,\ 0,\ 0,\ 0,\ 0,\ 0), \tag{28c}$$

$$r_4 = (0,\ 1,\ 0,\ 0,\ 0,\ 0,\ 0), \tag{28d}$$

$$r_5 = (0,\ 0,\ 0,\ 0,\ 1,\ 0,\ 0), \tag{28e}$$

$$r_6 = (0,\ 0,\ 0,\ 0,\ 0,\ 1,\ 0), \tag{28f}$$

$$r_7 = (0,\ 0,\ 0,\ 0,\ 0,\ 0,\ 1). \tag{28g}$$

The system is not strictly hyperbolic because u is a fivefold eigenvalue. On the other hand, the set of eigenvectors is complete, so no parabolic degeneracy exists. The wave fields associated with λ_1 and λ_2 are genuinely non-linear, whereas the wave fields associated with $\lambda_{3,4,5,6,7}$ are linearly degenerate. Physically, this means that λ_1 and λ_2 are associated with shocks or rarefactions, whereas $\lambda_{3,4,5,6,7}$ are associated with coinciding contact discontinuities.

Before we proceed to determine the relations that hold across shocks, rarefactions and contact discontinuities, it is interesting to examine the influence of the solid volume fraction on the mixture speed of sound c. If both phases obey a stiffened gas equation of state, Eq. (26) reduces to

$$c^2 = \frac{\gamma_g(p + P_g)}{\rho} \frac{\gamma_s - 1}{\phi_g(\gamma_s - 1) + \phi_s(\gamma_g - 1)}. \tag{29}$$

Fig. 5 shows the variation of the mixture speed of sound with the gas volume fraction for the present model (20) and for the system (6), for a particular set of physical parameters. As mentioned in [15],the mixture speed of sound corresponding to (6) is in good agreement with those measured experimentally for many heterogeneous mixtures with stiff mechanical relaxation. Further, from Fig. 5 it can be inferred that the mixture sound speeds for both the system (6) and the proposed conservative approximation (20) are very close at low and

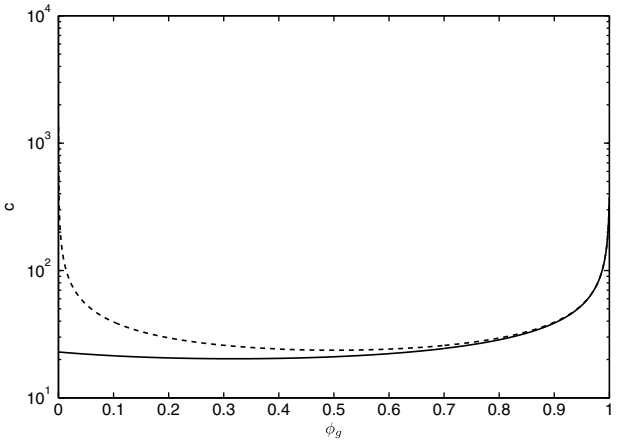

Fig. 5. Mixture speed of sound for the model of Kapila et al. [15] (dashed line) and the present model (solid line). The physical parameters are set at: $\gamma_g = 1.4$, $\gamma_s = 2.5$, $P_g = 0$, $P_s = 13 \times 10^8$ Pa, $\rho_g = 1$ kg/m^3, $\rho_s = 1000$ kg/m^3 and $p = 10^5$ Pa.

medium solid volume fractions. For example, for $\phi_s = 0.3$, the relative difference in the predictions of c is about 5%. On the other hand, at very dense mixtures, we observe large differences between the mixture sound speeds, as predicted by the two models. Such a behaviour is in agreement with the analysis of the validity limit of the conservative approximation that was given in the previous section. We mention here that in the numerical simulations presented in this article, the solid volume fractions will always be kept smaller than 0.3.

3.2. Rankine–Hugoniot relations across a shock

Since the balance equations are in conservative form, the Rankine–Hugoniot relations for the homogeneous part of Eqs. (20) can be derived in a straightforward manner. The result is

$$\phi_g^* \rho_g^* (u^* - w) = \phi_{g0} \rho_{g0} (u_0 - w), \tag{30a}$$
$$\phi_s^* \rho_s^* (u^* - w) = \phi_{s0} \rho_{s0} (u_0 - w), \tag{30b}$$
$$\rho^* u^* (u^* - w) + p^* = \rho_0 u_0 (u_0 - w) + p_0, \tag{30c}$$
$$\rho^* e_t^* (u^* - w) + p^* u^* = \rho_0 e_{t0} (u_0 - w) + p_0 u_0, \tag{30d}$$
$$\phi_s^* (u^* - w) = \phi_{s0} (u_0 - w), \tag{30e}$$
$$\phi_g^* \rho_g^* z^* (u^* - w) = \phi_{g0} \rho_{g0} z_0 (u_0 - w), \tag{30f}$$
$$N_s^* (u^* - w) = N_{s0} (u_0 - w), \tag{30g}$$

where the suffix "0" denotes the unshocked state, the exponent "$*$" denotes the shocked state and w is the shock speed. By defining the solid mass fraction, $Y_s \equiv (\phi_s \rho_s / \rho)$ and the gaseous mass fraction $Y_g \equiv (\phi_g \rho_g / \rho)$, these equations may be written in the following form:

$$m \equiv \rho^* (u^* - w) = \rho_0 (u_0 - w), \tag{31a}$$
$$Y_s^* = Y_{s0}, \tag{31b}$$
$$p^* - p_0 + m^2 (v^* - v_0) = 0, \tag{31c}$$
$$e^* - e_0 + \frac{p^* + p_0}{2} (v^* - v_0) = 0, \tag{31d}$$
$$z^* = z_0, \tag{31e}$$
$$\frac{\phi_s^*}{\rho^*} = \frac{\phi_{s0}}{\rho_0}, \tag{31f}$$
$$\frac{N_s^*}{\rho^*} = \frac{N_{s0}}{\rho_0}. \tag{31g}$$

Henceforth, we use the fact that the gas and solid phases obey a stiffened gas equation of state. The combination of (31b) and (31f) yields

$$\rho_{\mathrm{s}}^{*} = \rho_{\mathrm{s}0}. \tag{32}$$

Expanding (31d) by using (13), (31b) and (32) yields

$$v_{\mathrm{g}}^{*} = \frac{Y_{\mathrm{g}0} v_{\mathrm{g}0} \left(\frac{p_0 + \gamma_{\mathrm{g}} P_{\mathrm{g}}}{\gamma_{\mathrm{g}} - 1} + \frac{p_0 + p^{*}}{2} \right) + Y_{\mathrm{s}0} v_{\mathrm{s}0} \frac{p_0 - p^{*}}{\gamma_{\mathrm{s}} - 1}}{Y_{\mathrm{g}0} \left(\frac{p^{*} + \gamma_{\mathrm{g}} P_{\mathrm{g}}}{\gamma_{\mathrm{g}} - 1} + \frac{p_0 + p^{*}}{2} \right)}, \tag{33}$$

where $v_\alpha = \rho_\alpha^{-1}$ is the specific volume of phase $\alpha = g, s$

To determine the shocked state, we proceed in the following way. If the unshocked state and p^* are known, then Eqs. (31) and (32) yield

$$Y_{\mathrm{g}}^{*} = Y_{\mathrm{g}0}, \tag{34}$$

$$Y_{\mathrm{s}}^{*} = Y_{\mathrm{s}0}, \tag{35}$$

$$\rho_{\mathrm{s}}^{*} = \rho_{\mathrm{s}0}, \tag{36}$$

$$z^{*} = z_0. \tag{37}$$

Subsequently, v_{g}^{*} is computed by (33). Then the specific volume of the mixture in the shocked (downstream) state is given by $v^{*} = Y_{\mathrm{g}}^{*} v_{\mathrm{g}}^{*} + Y_{\mathrm{s}}^{*} / \rho_{\mathrm{s}}^{*}$. This allows the calculation of the downstream solid volume fraction

$$\phi_{\mathrm{s}}^{*} = \frac{\phi_{\mathrm{s}0}}{\rho_0 v^{*}} \tag{38}$$

and of the mass flux, cf. (31)

$$m = \pm \sqrt{\frac{p_0 - p^{*}}{v^{*} - v_0}}, \tag{39}$$

where the sign depends on the characteristic field. For a λ_1 shock, the negative sign has to be chosen, whereas for a λ_2 shock, the positive sign has to be chosen. The shock speed is then written as

$$w = u_0 - m v_0. \tag{40}$$

Finally, with the aid of (31a) and (40) we get

$$u^{*} = m v^{*} + w. \tag{41}$$

3.3. Riemann invariants

We now proceed to calculate the Riemann invariants, which correspond to the conserved quantities across rarefaction waves and contact discontinuities. Since there is no characteristic length or time scale in the homogeneous part of the governing system, the Riemann problem is self-similar, i.e., rarefactions and contact discontinuities are straight lines in the $x - t$ plane. This implies that these waves represent solutions of the system of interest in the form of $f(\xi \equiv x - wt)$, with w being the speed of the rarefaction waves or contact discontinuities. If such a change of variable is introduced, the governing equations become

$$(u-w)\frac{\mathrm{d}Y_\mathrm{s}}{\mathrm{d}\xi}=0, \tag{42a}$$

$$(u-w)\frac{\mathrm{d}\rho}{\mathrm{d}\xi}+\rho\frac{\mathrm{d}u}{\mathrm{d}\xi}=0, \tag{42b}$$

$$(u-w)\frac{\mathrm{d}u}{\mathrm{d}\xi}+\frac{1}{\rho}\frac{\mathrm{d}p}{\mathrm{d}\xi}=0, \tag{42c}$$

$$(u-w)\frac{\mathrm{d}p}{\mathrm{d}\xi}+\rho c^2\frac{\mathrm{d}u}{\mathrm{d}\xi}=0, \tag{42d}$$

$$(u-w)\frac{\mathrm{d}\phi_\mathrm{s}}{\mathrm{d}\xi}+\phi_\mathrm{s}\frac{\mathrm{d}u}{\mathrm{d}\xi}=0, \tag{42e}$$

$$(u-w)\frac{\mathrm{d}z}{\mathrm{d}\xi}=0, \tag{42f}$$

$$(u-w)\frac{\mathrm{d}N_\mathrm{s}}{\mathrm{d}\xi}+N_\mathrm{s}\frac{\mathrm{d}u}{\mathrm{d}\xi}=0. \tag{42g}$$

In the case of a contact discontinuity, $w=u$. Then, the above equations yield

$$u^*=u_0, \tag{43}$$

$$p^*=p_0, \tag{44}$$

where the suffix "0" denotes the downstream state and the exponent "$*$" denotes the upstream state of the contact discontinuity.

In the case of a rarefaction, $w=u\pm c$, and Eqs. (42) become

$$\mathrm{d}Y_\mathrm{s}=0, \tag{45a}$$

$$\frac{\mathrm{d}\rho}{\rho}=\pm\frac{\mathrm{d}u}{c}, \tag{45b}$$

$$\mathrm{d}p=\pm\rho c\,\mathrm{d}u, \tag{45c}$$

$$\frac{\mathrm{d}\phi_\mathrm{s}}{\phi_\mathrm{s}}=\pm\frac{\mathrm{d}u}{c}, \tag{45d}$$

$$\mathrm{d}z=0, \tag{45e}$$

$$\frac{\mathrm{d}N_\mathrm{s}}{N_\mathrm{s}}=\pm\frac{\mathrm{d}u}{c}. \tag{45f}$$

It should be mentioned that Eq. (42d), not rewritten here, has become identical with Eq. (42c). Some simple manipulations of (45) lead to

$$\mathrm{d}Y_\mathrm{s}=0, \tag{46a}$$

$$\frac{\mathrm{d}\rho}{\rho}=\frac{\mathrm{d}\phi_\mathrm{s}}{\phi_\mathrm{s}}, \tag{46b}$$

$$\mathrm{d}p=\pm\rho c\,\mathrm{d}u, \tag{46c}$$

$$\frac{\mathrm{d}\phi_\mathrm{s}}{\phi_\mathrm{s}}=\frac{\mathrm{d}p}{\rho c^2}, \tag{46d}$$

$$\mathrm{d}z=0, \tag{46e}$$

$$\frac{\mathrm{d}N_\mathrm{s}}{N_\mathrm{s}}=\frac{\mathrm{d}\phi_\mathrm{s}}{\phi_\mathrm{s}}. \tag{46f}$$

which are the equations we integrate in order to obtain the Riemann invariants relative to a rarefaction. First, the combination of (29) in (46d) gives

$$\frac{\mathrm{d}p}{p+P_\mathrm{g}}=\frac{\gamma_\mathrm{g}(\gamma_\mathrm{s}-1)}{\phi_\mathrm{s}(\phi_\mathrm{s}(\gamma_\mathrm{g}-\gamma_\mathrm{s})+(\gamma_\mathrm{s}-1))}\mathrm{d}\phi_\mathrm{s}, \tag{47}$$

which can be integrated analytically. The result is

$$\phi_s^* = \frac{\frac{\phi_{s0}(\gamma_s-1)}{(\gamma_g-\gamma_s)\phi_{s0}+(\gamma_s-1)}\left(\frac{p^*+P_g}{p_0+P_g}\right)^{\frac{1}{\gamma_g}}}{1-\frac{(\gamma_g-\gamma_s)\phi_{s0}}{(\gamma_g-\gamma_s)\phi_{s0}+(\gamma_s-1)}\left(\frac{p^*+P_g}{p_0+P_g}\right)^{\frac{1}{\gamma_g}}}. \tag{48}$$

On the other hand, Eqs. (46a), (46b), (46e) and (46f) give, upon integration,

$$Y_s^* = Y_{s0}, \tag{49}$$

$$\rho^* = \rho_0 \frac{\phi_s^*}{\phi_{s0}}, \tag{50}$$

$$z^* = z_0, \tag{51}$$

$$N_s^* = N_{s0} \frac{\phi_s^*}{\phi_{s0}}. \tag{52}$$

Finally, from (29) and (48) it can be shown that

$$\rho c = \sqrt{\frac{\gamma_g(\gamma_s-1)\rho_0}{(\gamma_g-\gamma_s)\phi_{s0}+(\gamma_s-1)} \frac{(p+P_g)^{\frac{\gamma_g+1}{\gamma_g}}}{(p_0+P_g)^{\frac{1}{\gamma_g}}}}. \tag{53}$$

Introducing this result in (46c) and upon integration we obtain

$$(u^*-u_0) = \pm\frac{2\gamma_g}{\gamma_g-1}\sqrt{\frac{\left((\gamma_g-\gamma_s)\phi_{s0}+(\gamma_s-1)(p_0+P_g)^{\frac{1}{\gamma_g}}\right)}{\gamma_g(\gamma_s-1)\rho_0}}\left((p^*+P_g)^{\frac{\gamma_g-1}{2\gamma_g}}-(p_0+P_g)^{\frac{\gamma_g-1}{2\gamma_g}}\right). \tag{54}$$

To determine the upstream state of a rarefaction, we proceed as follows. Let us assume that all downstream variables and p^* are known. Then, the solid volume fraction and the velocity are calculated from Eqs. (48) and (54), respectively. All other variables can then be calculated with Eqs. (49)–(52).

3.4. Exact solution of the Riemann problem

In this section, we briefly describe the numerical method employed to solve in an exact way the Riemann problem associated with the homogeneous part of system (20). This method is based on the solver of Colella and Glaz [20] for the gasdynamic Euler equations.

Consider an initial discontinuity separating two uniform states, denoted by L (for "left") and R (for "right"). At later times three different waves will be developed, see Fig. 6. The middle wave, separating the new intermediate states (denoted by 1 and 2) will always be a contact discontinuity moving at the mixture's velocity, whereas the left and right waves can be either shocks or rarefactions. Given initial left and right states, the objective is to calculate the speeds of these waves and the state variables in regions 1 and 2.

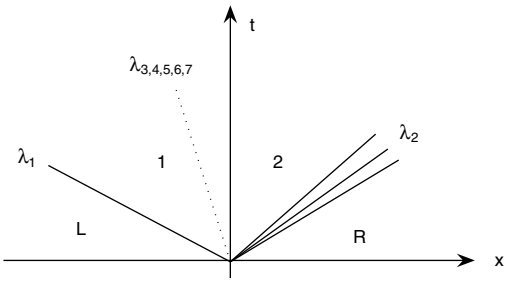

Fig. 6. Graphic representation of the solution of the Riemann problem. Waves λ_1 and λ_2 can be shocks or rarefactions.

To this end, let us assume that the pressure in region 1 is also known. Then, we may calculate all other variables in region 1 by employing the relations that hold across the left wave. In particular, if $p_1 > p_L$, we use the Rankine–Hugoniot relations for a shock (33)–(41), otherwise we use the relations for a rarefaction (48)–(54). Next, across the contact discontinuity, the pressure is conserved, see Eq. (44), so $p_2 = p_1$. Then, in a similar manner as for region 1, we may also calculate all other variables in region 2. Indeed, if $p_2 > p_R$, we use the Rankine–Hugoniot relations for a shock, otherwise we use the relations for a rarefaction.

Thus, the solution can be parametrized with respect to p_1 (which was initially assumed as known). In other words, we can set up an iterative procedure based on p_1 to compute the solution to the Riemann problem. The criterion of convergence is the velocity u_2, because there are two ways to compute this variable. The first way is via Eq. (43) once the state of region 1 has been calculated. The second way is via the relations that hold across the right wave. This iteration terminates once the two different numerical predictions for u_2 become equal. In summary, the iterative procedure works as follows,

i. Given an estimate of p_1, the flow variables in region 1 are calculated via (33)–(41) if $p_1 > p_L$, or via (48)–(54) if $p_1 \leqslant p_L$.
ii. Next, p_2 is set at $p_2 = p_1$, by virtue of (44).
iii. Next, the flow variables in region 2 are calculated via (33)–(41) if $p_2 > p_R$, or via, (48)–(54) if $p_2 \leqslant p_R$.
iv. The iteration has converged if $u_1 = u_2$ (within a prescribed precision).

4. Steady-wave analysis for two-phase detonations

In this section, we focus on the study of the steady-wave structures of 1D two-phase detonations described by the proposed approximate model. This analysis is similar to the ZND analysis of gaseous detonations, see [21].

4.1. Steady-wave profile

Let us consider a steady detonation propagating to the right with speed D, through a quiescent two-phase medium, denoted by the suffix 0. In the reference frame of the precursor shock, this is equivalent to consider a stationary shock, into which the quiescent medium flows with speed $u_0 = -D$. In order to determine the profiles of the flow variables along the steady detonation, we set the time derivatives of (20) equal to zero. Assuming that the precursor shock is located at $x = 0$, we have, for each $x < 0$,

$$\frac{\mathrm{d}}{\mathrm{d}x}(\phi_{\mathrm{g}}\rho_{\mathrm{g}}u) = M, \tag{55a}$$

$$\frac{\mathrm{d}}{\mathrm{d}x}(\phi_{\mathrm{s}}u) = S, \tag{55b}$$

$$\frac{\mathrm{d}}{\mathrm{d}x}(\phi_{\mathrm{g}}\rho_{\mathrm{g}}uz) = Q, \tag{55c}$$

$$\rho u = \rho_0 u_0, \tag{55d}$$

$$\rho_0 u_0^2 + p_0 = \rho u^2 + p, \tag{55e}$$

$$\left(\phi_{\mathrm{g}0}\frac{p_0+\gamma_{\mathrm{g}}P_{\mathrm{g}}}{\gamma_{\mathrm{g}}-1} + \phi_{\mathrm{s}0}\frac{p_0+\gamma_{\mathrm{s}}P_{\mathrm{s}}}{\gamma_{\mathrm{s}}-1} + \frac{\rho_0 u_0^2}{2} + \phi_{\mathrm{g}0}\rho_{\mathrm{g}0}q_{\mathrm{g}}z_0 + \phi_{\mathrm{s}0}\rho_{\mathrm{s}0}q_{\mathrm{s}} + p_0\right)u_0$$
$$= \left(\phi_{\mathrm{g}}\frac{p+\gamma_{\mathrm{g}}P_{\mathrm{g}}}{\gamma_{\mathrm{g}}-1} + \phi_{\mathrm{s}}\frac{p+\gamma_{\mathrm{s}}P_{\mathrm{s}}}{\gamma_{\mathrm{s}}-1} + \frac{\rho u^2}{2} + \phi_{\mathrm{g}}\rho_{\mathrm{g}}q_{\mathrm{g}}z + \phi_{\mathrm{s}}\rho_{\mathrm{s}}q_{\mathrm{s}} + p\right)u, \tag{55f}$$

$$N_0 u_0 = N u, \tag{55g}$$

where M, Q and S are, respectively, given by (7,12) and (19). This is a system of Differential Algebraic Equations (DAE). By integrating the differential equations of this system and inserting the result in (55f), we get, after some algebra,

$$
\begin{aligned}
&-u^2\frac{\rho_0 u_0}{2}\left(\frac{\gamma_g+1}{\gamma_g-1}\right)+u\left(\frac{\gamma_g}{\gamma_g-1}(p_0+P_g+\rho_0u_0^2)+\rho_0u_0\left(\frac{1}{\gamma_s-1}-\frac{1}{\gamma_g-1}\right)\left(\int_x^0 S\,dx-\phi_{s0}u_0\right)\right)\\
&\quad+q_s\int_x^0 M\,dx-q_g\int_x^0 Q\,dx+\left(\frac{1}{\gamma_s-1}-\frac{1}{\gamma_g-1}\right)\left(\phi_{s0}\rho_0u_0^3-(p_0+\rho_0u_0^2)\int_x^0 S\,dx\right)\\
&\quad-\left(\frac{\gamma_sP_s}{\gamma_s-1}-\frac{\gamma_gP_g}{\gamma_g-1}\right)\int_x^0 S\,dx-u_0\frac{\gamma_g}{\gamma_g-1}(p_0+P_g)-\frac{\rho_0u_0^3}{2}=0.
\end{aligned}
\tag{56}
$$

The profile of the two-phase detonations can then numerically be computed in the following way. Starting from the point just behind the shock and advancing through the reaction region, we calculate at each x, progressively,

i. the velocity u from relation (56),
ii. the solid volume fraction ϕ_s from (55b),
iii. the gaseous density ρ_g from (55a),
iv. the solid density ρ_s from (55d),
v. the pressure p from (55e),
vi. the mass reactant fraction z from (55c),
vii. the particle number density N_s with (55g),

where the integrals appearing in (56) are approximated numerically from the values of the flow variables as calculated at the preceding points.

Since relation (56) is a quadratic equation for u, we must select the physically relevant solution. To this end, let us consider the point just behind the shock, so that the integrations of the source terms S, Q and M are still zero. The velocity of the mixture at this point is given by

$$
\begin{aligned}
&-u^2\frac{\rho_0 u_0}{2}\left(\frac{\gamma_g+1}{\gamma_g-1}\right)+u\left(\frac{\gamma_g}{\gamma_g-1}(p_0+P_g+\rho_0u_0^2)-\rho_0u_0\left(\frac{1}{\gamma_s-1}-\frac{1}{\gamma_g-1}\right)\phi_{s0}u_0\right)\\
&\quad+\left(\frac{1}{\gamma_s-1}-\frac{1}{\gamma_g-1}-\frac{1}{2}\right)\phi_{s0}\rho_0u_0^3-u_0\frac{\gamma_g}{\gamma_g-1}(p_0+P_g)=0
\end{aligned}
\tag{57}
$$

and thus

$$
u=\frac{\frac{\gamma_g}{\gamma_g-1}(p_0+P_g+\rho_0u_0^2)-\rho_0u_0\left(\frac{1}{\gamma_s-1}-\frac{1}{\gamma_g-1}\right)\phi_{s0}u_0\pm\sqrt{\xi}}{\rho_0u_0\frac{\gamma_g+1}{\gamma_g-1}},
\tag{58}
$$

where ξ is the discriminant of (57),

$$
\xi=\left((p_0+P_g)\frac{\gamma_g}{\gamma_g-1}-\rho_0u_0^2\left(\frac{\phi_{s0}}{\gamma_s-1}+\frac{\phi_{g0}}{\gamma_g-1}\right)\right)^2.
\tag{59}
$$

The Lax shock-admissibility criterion implies that $u+c>0>u_0+c_0$. Since $u_0=-D<0$, this also means that $(c_0)^2<u_0^2$. By virtue of (29), this inequality can be written as

$$
(p_0+P_g)\frac{\gamma_g}{\gamma_g-1}-\rho_0u_0^2\left(\frac{\phi_{s0}}{\gamma_s-1}+\frac{\phi_{g0}}{\gamma_g-1}\right)<0.
\tag{60}
$$

Then, from (59) and (60) it follows that

$$\sqrt{\xi} = -(p_0 + P_g)\frac{\gamma_g}{\gamma_g - 1} + \rho_0 u_0^2\left(\frac{\phi_{s0}}{\gamma_s - 1} + \frac{\phi_{g0}}{\gamma_g - 1}\right). \tag{61}$$

Further, if we chose the negative sign in Eq. (58) the expression of u simply reduces to $u = u_0$, which implies that there is no jump at $x = 0$. Therefore the physically relevant solution is the one with the positive sign.

4.2. Minimum detonation speed

It is important to note that a steady detonation can be calculated only if the quadratic equation (56) admits a solution *for each* x. Obviously, a solution exists if the discriminant ξ of (56) is greater or equal to zero. This discriminant depends on the downstream state and on the material specific constants, but also on the values of S, M and Q along the detonation profile. In general, it is very difficult to see a priori if a steady-wave solution exists. Nevertheless, in some cases, we can determine a lower limit for the speed of propagation of the detonation, as done in the ZND theory.

Let us consider the case of reactive solid particles. If the solid temperature becomes sufficiently high behind the precursor shock, $T_s > T_{ign}$, and since we have assumed an ignition-type mechanism for the solid particle burning, the solid particles will have reacted completely at $x \to -\infty$ and therefore $\phi_s \to 0$. But at $x \to -\infty$ the gaseous reaction has also been completed. Then, the integrals in (56) reduce to

$$\int_{-\infty}^{0} M\,\mathrm{d}x = -\phi_{s0}\rho_{s0}u_0, \tag{62a}$$

$$\int_{-\infty}^{0} S\,\mathrm{d}x = \phi_{s0}u_0, \tag{62b}$$

$$\int_{-\infty}^{0} Q\,\mathrm{d}x = \phi_{g0}\rho_{g0}z_0u_0. \tag{62c}$$

Hence, at $x \to -\infty$, the discriminant of (56) becomes

$$\begin{aligned}\xi = {} & \left(\frac{\gamma_g}{\gamma_g - 1}(p_0 + P_g + \rho_0 u_0^2)\right)^2 + 4\frac{\rho_0 u_0}{2}\left(\frac{\gamma_g + 1}{\gamma_g - 1}\right)\left(-\phi_{s0}\rho_{s0}u_0q_s - \phi_{g0}\rho_{g0}u_0z_0q_g\right. \\ & + \left(\frac{1}{\gamma_s - 1} - \frac{1}{\gamma_g - 1}\right)\left(\phi_{s0}\rho_0u_0^3 - \phi_{s0}u_0(p_0 + \rho_0u_0^2)\right) - \phi_{s0}u_0\left(\frac{\gamma_sP_s}{\gamma_s - 1} - \frac{\gamma_gP_g}{\gamma_g - 1}\right) \\ & \left. -u_0\frac{\gamma_g}{\gamma_g - 1}(p_0 + P_g) - \frac{\rho_0u_0^3}{2}\right).\end{aligned} \tag{63}$$

But for Eq. (56) to have a solution at $x \to -\infty$, it is necessary that the discriminant be non-negative. Therefore, after rearranging (63), the following condition should hold

$$\begin{aligned}& u_0^4\rho_0^2 + 2\rho_0u_0^2(-\gamma_g(p_0 + P_g) - \phi_{s0}\rho_{s0}(\gamma_g^2 - 1)q_s - \phi_{g0}\rho_{g0}z_0(\gamma_g^2 - 1)q_g \\ & - \phi_{s0}(\gamma_g^2 - 1)\left(\frac{p_0 + \gamma_sP_s}{\gamma_s - 1} - \frac{p_0 + \gamma_gP_g}{\gamma_g - 1}\right)) + \gamma_g^2(p_0 + P_g)^2 \geqslant 0.\end{aligned} \tag{64}$$

For given material constants and for given state ahead of the shock, this inequality becomes a condition on $u_0 = -D$, i.e., the detonation propagation speed. The left-hand side of this inequality is a quadratic polynomial for u_0^2. Therefore the minimum value of u_0^2 that satisfies (64) is

$$u_{0\min}^2 = a + \sqrt{b}, \tag{65}$$

with

$$a \equiv \frac{\gamma_g(p_0+P_g)+(\gamma_g^2-1)\left(\phi_{s0}\rho_{s0}q_s+\phi_{g0}\rho_{g0}z_0q_g+\phi_{s0}\left(\frac{p_0+\gamma_sP_s}{\gamma_s-1}-\frac{p_0+\gamma_gP_g}{\gamma_g-1}\right)\right)}{\rho_0}, \tag{66}$$

$$b \equiv a^2-\frac{\gamma_g^2(p_0+P_g)^2}{\rho_0^2}. \tag{67}$$

It follows that

$$-u_0 = D > \sqrt{a+\sqrt{b}}. \tag{68}$$

We note that the minimum speed reduces to the Chapman–Jouguet velocity for gaseous detonations when the solid volume fraction ϕ_{s0} tends to zero.

It is also important to mention that (68), derived by assuming complete burning of the solid particles, is a necessary condition for the existence of steady detonations. In some cases, but not always, it is also a sufficient condition. In particular, if S is zero then (68) is also sufficient. To demonstrate this, we first note that since both reactions (1) and (2) are irreversible, then both $\int_x^0 M\,dx$ and $-\int_x^0 Q\,dx$ are monotonic (increasing with decreasing x). It follows that the discriminant ξ of (56) is also monotonic, and decreasing with decreasing x. Then, the most restrictive, i.e., the smallest value of ξ, would indeed be at $x \to -\infty$, which rends (68) a necessary and sufficient condition for existence of solution of the steady-wave equations. On the other hand, when S is not zero, and since $\int_x^0 S\,dx$ is not necessarily monotonic, such a conclusion cannot be deduced. In that case, a condition more restrictive than (68) may exist at another location, $-\infty < x < 0$.

Finally, we mention that when the solid particles are inert the above analysis cannot be performed. In that case it is impossible to predict the values of the solid volume fraction and the velocity at the end of the two-phase detonation. This does not allow the calculation of $\int_{-\infty}^0 S\,dx$ in (55e). On the other hand, we have observed numerically that steady two-phase detonation could exist and propagate at constant speeds that are lower than the corresponding Chapman–Jouguet speed D_{CJ} for gaseous detonations.

4.3. Description of some steady two-phase detonation profiles

In this section, we present some typical steady two-phase detonation profiles, propagating with speed D through a mixture of reactive or inert solid particles. As usual, the overdrive factor of the detonation is given by $f = (D/D_{CJ})^2$ where D_{CJ} is the Chapman–Jouguet velocity of the corresponding gaseous detonation. For gaseous detonations, we always have $f \geqslant 1$. This is not necessarily true for two-phase detonations.

Pressure, density and temperature variables are non-dimensionalized with respect to the corresponding values of the gas in the quiescent medium, while the half-reaction length, $L_{1/2}$, i.e., the distance between the precursor shock and the point where $z = 0.5$, has been used as unit length. The values of the material-specific constants are taken as

$$\gamma_g = 1.2, \quad P_g = 0, \quad \gamma_s = 4.22, \quad P_s = 3.24 \times 10^5.$$

The state variables in the quiescent medium are

$$p_g = p_s = 1, \quad \rho_g = 1, \quad \rho_s = 8050.$$

The reaction-parameters for the gaseous reaction are set to

$$K_g = 230.75, \quad q_g = 50, \quad E_{ag} = 50.$$

The above values correspond to a gaseous ZND detonation of overdrive factor $f = 1.6$. The value of the (non-dimensional) gaseous heat capacity is $c_{v,g} = 1/(\gamma_g - 1)$, while the solid heat capacity is set to $c_{v,s} = 2.5\,c_{v,g}$.

Finally, in the calculation of the heat transfer coefficient H in (10), c_{pg} is determined by $c_{pg} = \gamma_g c_{v,g}$. We also set $Pr = 0.75$, $\mu_0 = 10^{-5}$.

4.3.1. Case A: inert particles

Since the particles are assumed to be inert, then $K_s = 0$ and $q_s = 0$. In the quiescent medium ahead of the shock the particles have a diameter of $d_s = 10^{-3}$ and the solid volume fraction is $\phi_s = 10^{-4}$.

Figs. 7–9 show profiles of the pressure, temperatures and solid volume fraction, respectively, for the two-phase detonation and the corresponding gaseous detonation propagating at the same speed. In Figs. 7 and 8 we observe that the presence of solid particles in the reactive medium yields a much higher post-shock pressure and gaseous temperature. This leads to a faster burning of the reactive gas ($z = 0.5$ at $x = -0.1\,L_{1/2}$), instead of $x = -L_{1/2}$ in the corresponding gaseous detonation. Therefore, the reaction is concentrated in a very thin zone right behind the shock. Inside this zone the pressure drops as the gas accelerates, as well as the solid volume fraction. The thin reaction zone is then followed by a large region inside which heat is transferred from the hot burnt gas to the particles. The two phases reach thermal equilibrium at $T = 3.41$, quite lower than in the corresponding gaseous detonation.

We observe that, even at low particle concentrations, the pressure behind the shock is much higher than the pressure field of purely gaseous detonations. The physical explanation for the increased pressures is the following. The primary effect of the particle addition is to increase the density of the mixture. For this reason, the density of the particulate phase is as significant a parameter as the volume fraction. Thus, it is better to

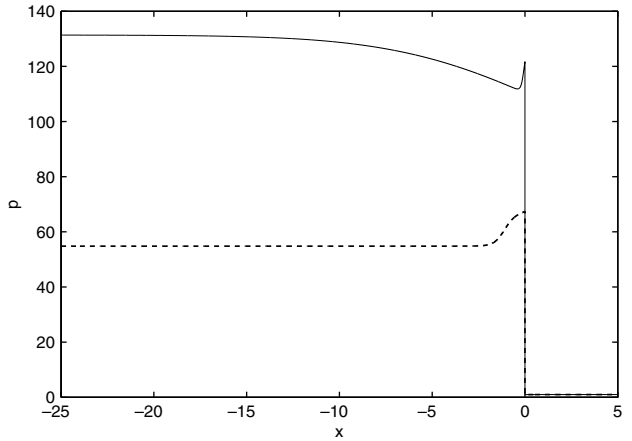

Fig. 7. Case A: pressure profiles for a steady two-phase detonation wave with inert particles (solid line) and the gaseous ZND wave at the same velocity (dashed line).

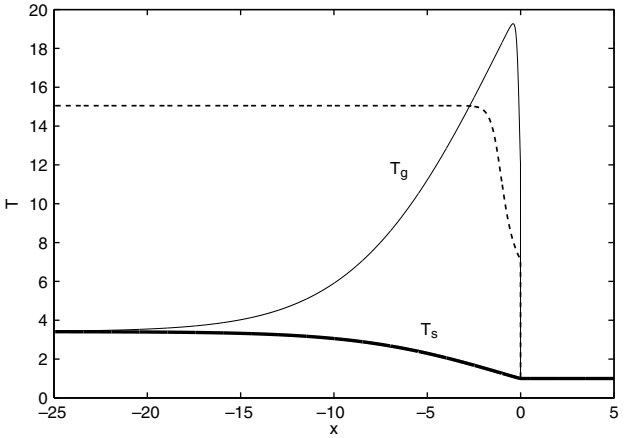

Fig. 8. Case A: steady-state temperature profiles for the two-phase detonation with inert particles (solid line) and the gaseous detonation propagating at the same velocity (dashed line). Gas variables are represented by thin lines and solid variables are represented by bold lines.

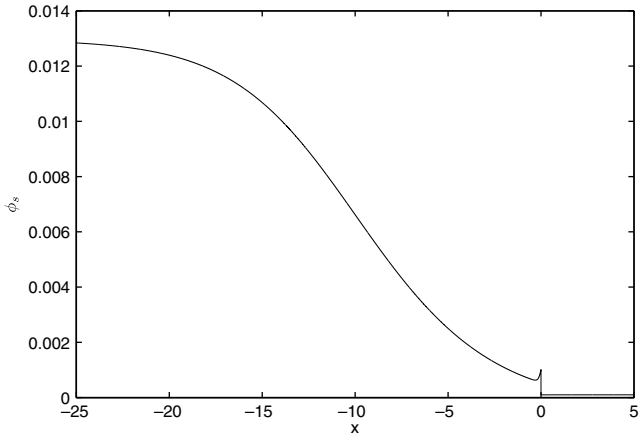

Fig. 9. Case A: steady-state solid volume fraction profile for the two-phase detonation with inert particles.

consider the partial density ($\rho_\alpha\phi_\alpha$) as the relevant physical quantity because it is the sum of the partial densities that equals the mixture density. Addition of few heavy particles has a profound effect on the mixture density. In this case, the partial densities of the two phases are approximately equal even though the solid volume concentration is small, $\rho_s\phi_s \simeq \rho_g\phi_g$. Thus, $\rho_s\phi_s + \rho_g\phi_g \simeq 2\rho_g\phi_g \simeq 2\rho_g$, since $\phi_g \simeq 1$. For such low concentrations, we can roughly approximate the jump across a shock propagating in this medium by the jump across a shock propagating in pure gas with density equal the density of our mixture, $2\rho_g$. In purely gaseous flows a doubling of the density ahead of the shock results in an increase of the post-shock pressure of the same order, when the shock speed remains the same. In the two-phase medium, the jump relations of our model predict the same behaviour: the larger the partial density of the solid phase is, the larger the post-shock pressure becomes under constant shock speed. This is precisely what Fig. 7 shows.

It is also worth mentioning that the heat transfer between the two phases results in an increase in the solid volume fraction, cf. (19) and (20e). This implies the formation of a compaction zone behind the detonation, due to thermal non-equilibrium between the two phases. The fact that thermal non-equilibrium alone can directly evolve the solid volume fraction has been predicted by the model of Papalexandris [7], whereas the Baer and Nunziato model [3] predicts that evolution of the solid volume fraction, in the absence of mass transfer between the two phases, can be produced by mechanical non-equilibrium only.

4.3.2. Case B: reactive particles

In this case, the solid particles of the mixture are considered as reactive. The parameters of the heterogeneous reaction are set to

$$K_s = 2 \times 10^{-7}, \quad q_s = 50, \quad T_{ign} = 2.$$

Moreover, in the quiescent medium ahead of the shock, the following values are set, $\phi_s = 5 \times 10^{-5}$ and $d_s = 10^{-3}$. The propagation speed of this steady detonation is $D = 8.66$, corresponding to an overdrive factor of $f = 1.6$. Given the above physical parameters, the minimum speed for a steady two-phase detonation, as determined by (68), is $D_{min} = 7.6$. This implies that minimum overdrive factor is $f_{min} = 1.27$.

Figs. 10–12 show profiles of the pressure, temperatures and solid volume fraction, respectively, for the two-phase detonation with reactive particles and the corresponding one with inert particles that propagates at the same speed. Right behind the shock, the profile of the detonation with reactive particles is identical to the one with inert particles. The high post-shock temperature results in fast burning of the gas with subsequent release of heat. Some of this heat is transferred to the particles. As a result, the solid temperature is slowly rising. Once it reaches the ignition temperature the particle begin to react.

So overall, the region behind the leading shock can be divided in three zones. The first one is the thin, about $0.25\,L_{1/2}$, gaseous reaction zone. A particle compaction area is formed due to momentum transfer from the gas to the solid particles. The second one, having a length of about $5\,L_{1/2}$, is the induction zone for the heterogeneous reaction, and is characterized by the heating-up of the particles by the hot burnt gas. In other words,

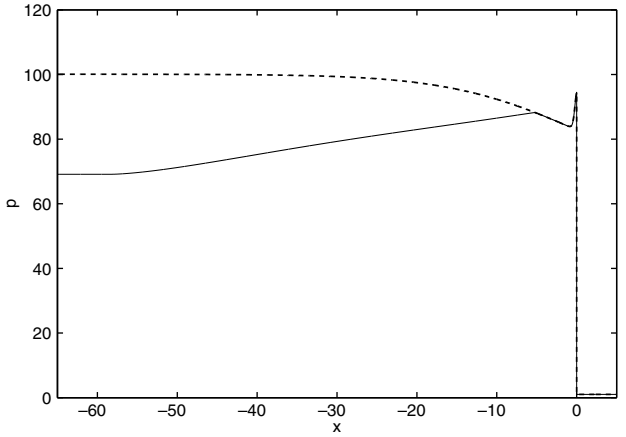

Fig. 10. Case B: steady-state pressure profiles for the two-phase detonation with reactive particles (solid line) and the corresponding two-phase detonation with inert particles (dashed line).

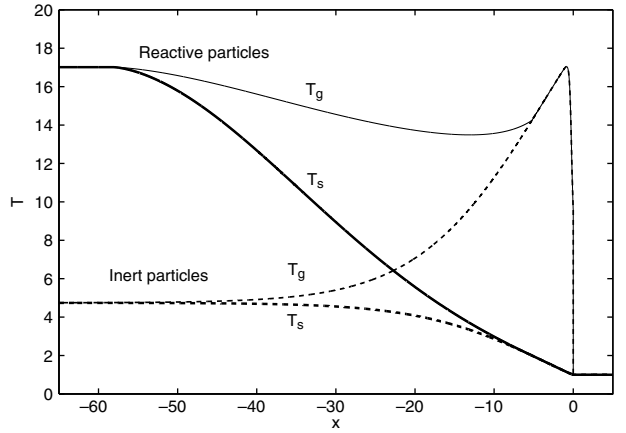

Fig. 11. Case B: steady-state temperature profiles for the two-phase detonation with reactive particles. Gas temperature is represented by thin line and solid temperature by bold line. The dashed line depicts the temperature field for the corresponding purely gaseous detonation.

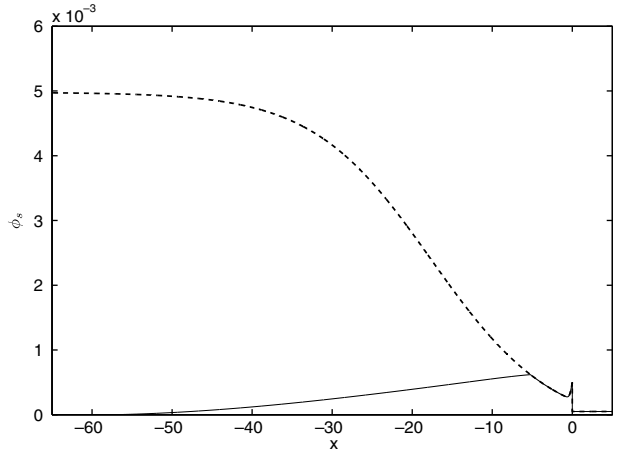

Fig. 12. Case B: steady-state solid volume fraction profiles for the two-phase detonation with reactive particles (solid line) and the corresponding two-phase detonation with inert particles (dashed line).

inside this zone the gas temperature drops and the solid temperature rises. This zone is also characterized by high values of particle concentration due to momentum transfer from the gaseous phase to the particulate one. In other words, the particle compaction area that was developed in the first zone extends to the second zone also.

The third zone is the particle burning zone and is approximatively 55 $L_{1/2}$ long. Since the particles do not burn as fast as the gas does, the length of this zone is much longer than the one of the first zone. It is interesting to mention that the product of this heterogeneous reaction is hot gas. Therefore, the temperature of the gaseous phase increases as the reaction proceeds. The temperature of the particles is then increased also via the heat transfer mechanism between the two phases. The two phases reach thermal equilibrium near the end of this zone. Beyond this zone, the medium consists of hot burnt gases only.

5. Numerical results and discussion

In this section, we present results of one-dimensional simulations and a preliminary two-dimensional simulation, based on the proposed conservative approximation. The algorithm that we employed in these simulations is the unsplit scheme for hyperbolic conservation laws with source terms proposed by Papalexandris et al. [22,23]. According to this approach, all convective and source terms are integrated simultaneously, without time splitting. As in the previous section, pressure, density and temperature variables are non-dimensionalized with respect to the corresponding values of the gas in the quiescent medium, while the half-reaction length, $L_{1/2}$, i.e., the distance between the precursor shock and the point where $z = 0.5$, has been used as unit length.

5.1. One-dimensional numerical simulations

We consider a gaseous ZND detonation that impacts a quiescent heterogeneous mixture, located at $x = 500\,L_{1/2}$, containing inert (Case C) or reactive particles (Case D). We perform the simulations in the frame of the laboratory. Therefore, inflow conditions are imposed on the left boundary, while outflow conditions are imposed on the right boundary. As in the previous section, the material specific constants are

$$\gamma_g = 1.2, \quad P_g = 0, \quad \gamma_s = 4.22, \quad P_s = 3.24 \times 10^5.$$

In the quiescent medium, the variables are

$$p_g = p_s = 1, \quad \rho_g = 1, \quad \rho_s = 8050, \quad d_s = 0.001.$$

The gaseous reaction-parameters are set to

$$K_g = 230.75, \quad q_g = 50, \quad E_{ag} = 50.$$

These parameters correspond to a ZND wave of overdrive factor $f = 1.6$. The equivalent gaseous detonation has been studied extensively in the past; see, for example, Papalexandris et al. [22] and references therein. It represents a case of a pulsating detonation, that is, a detonation with one linearly unstable mode.

5.1.1. Case C: inert particles

In this case, the solid particles ahead of the shock have a volume fraction of $\phi_s = 10^{-3}$. Since they are assumed to be inert, we set $K_s = 0$ and $q_s = 0$. The spatial resolution of the simulation is 100 points per unit length. Numerical convergence studies have shown that this spatial resolution is sufficient to properly resolve all relevant scales of the flow field. The simulations are performed with a CFL = 0.5. The length of the computational domain is 1200 $L_{1/2}$.

Fig. 13 shows profiles of pressure at times $t = 40.0$ and $t = 170.0$, Figs. 14 and 15 show profiles of temperature, and solid volume fraction, respectively, at time $t = 170.0$, and Fig. 16 shows on an $x - t$ diagram the trajectory of the precursor shock. At $t = 40.0$ the detonation has not yet encountered the two-phase medium and pulsates with high pressure peaks. The maxima of the shock pressure exceed $p = 90$. The average speed of the detonation is, approximately, $D_{av} \approx 8.66$, which is close to the predicted ZND value. When the detonation reaches the contact line that separates the purely gaseous medium and the heterogeneous mixture it interacts

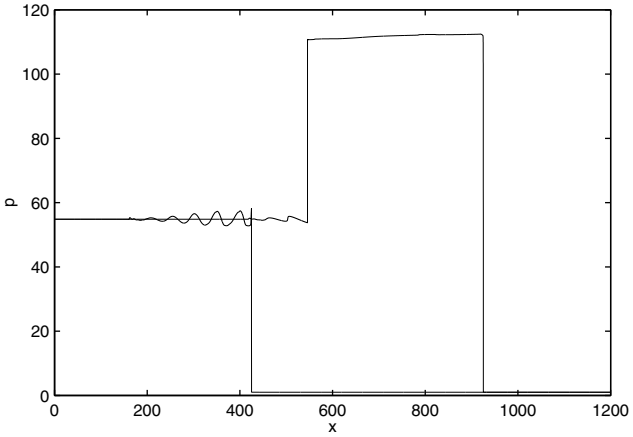

Fig. 13. Case C: pressure profiles of the transmission of a gaseous detonation to a two-phase mixture with inert particles at times $t = 40$ and $t = 170$.

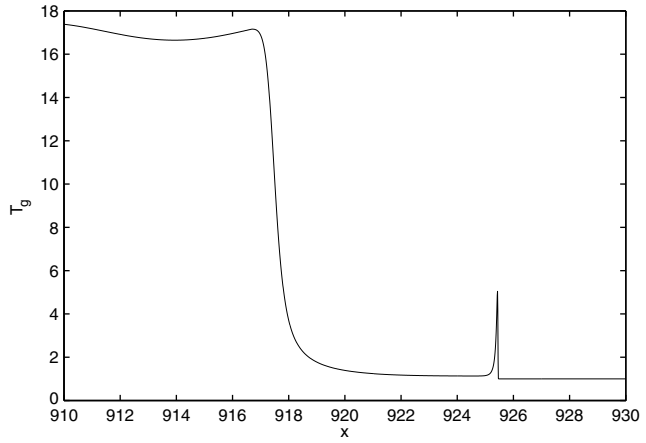

Fig. 14. Case C: gas temperature profile of the transmission of a gaseous detonation to a two-phase mixture with inert particles at time $t = 170$.

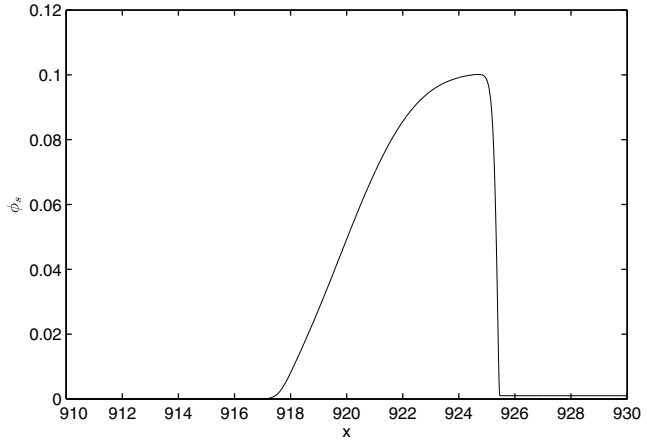

Fig. 15. Case C: solid volume fraction profile of the transmission of a gaseous detonation to a two-phase mixture with inert particles at time $t = 170$.

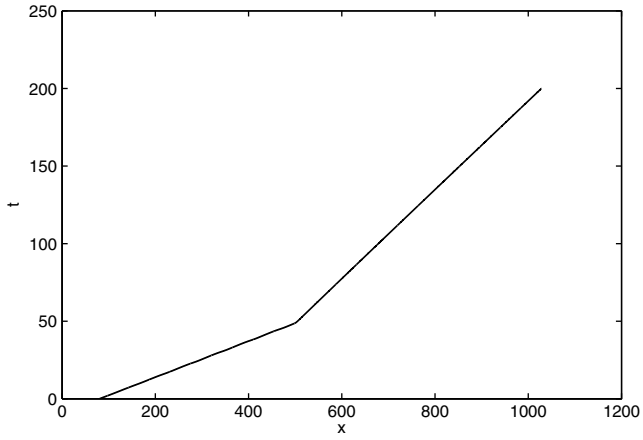

Fig. 16. Case C: $x - t$ diagram of the trajectory of the precursor shock.

with it, thus producing a transmitted detonation and a reflected inert shock. The post-shock pressure of the transmitted detonation is higher than the one predicted by the ZND theory for the initial gaseous detonation, $p \approx 112$, cf. Fig. 13. The strength of the precursor shock of the transmitted detonation remains constant with time, i.e., this is a case of a stable detonation. However, its speed is much lower than the one of the initial gaseous detonation, see Fig. 16. Indeed, after having encountered the two-phase medium, the propagation speed of the detonation rapidly decreases to $D \approx 3.5$. We therefore deduce that the inert solid particles tend to stabilize the detonation but they also decelerate the detonation speed.

In Fig. 15, we observe that behind the detonation wave the solid volume fraction increases. In other words, there is formation of a compaction zone. The formation of this compaction zone is due to the fact that the transmitted detonation "pulls" the solid particles with it, through the mechanism of mechanical relaxation. It is confined between the precursor shock and a contact discontinuity. As expected, this contact discontinuity moved at speed that is lower than the detonation speed. Therefore, the length of the particle compaction zone increases continuously. Finally, it is interesting to note that the profile of the transmitted detonation predicted by this simulation is in very good agreement with the equivalent steady-wave profile, cf. Section 4.3.

We have also performed a parametric study to explore the effect of the solid volume fraction in the quiescent mixture, ϕ_{s0}. Fig. 17 depicts the variation of the average propagation speed D_{av} of the transmitted detonation with respect to ϕ_{s0}. It is observed that D_{av} decreases monotonically with ϕ_s. The drop of D_{av} in the region of small ϕ_s is quite large, whereas at larger solid volume fractions the rate of decrease of D_{av} drops.

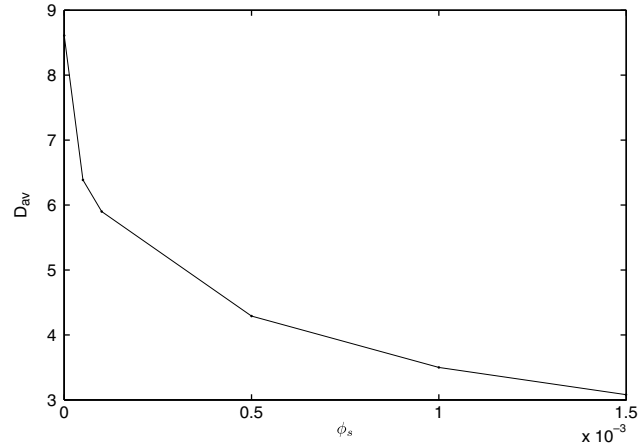

Fig. 17. Case C: variation of the average speed of propagation D_{av} with respect to the volume fraction of the solid particles.

A similar trend had been observed in the simulations presented in [9,10], which treated the case of incompressible solid particles.

A grid-convergence study for this case has also been performed. As criteria for numerical convergence we have used the average detonation speed, D_{av}, and a discrete version of the L_1 norm of the error in the prediction of the pressure. The average wave speed is a global quantity of detonating flows commonly used as a measure of the accuracy of simulations. The error of the average wave speed between $t = 100$ and $t = 200$, $|D_{\mathrm{ex}} - D_{\mathrm{av}}|/D_{\mathrm{ex}}$, is plotted against the grid resolution in Fig. 18. For $\hat{D}$ we have considered the average wave speed predicted by a simulation using a grid of 200 points/$L_{1/2}$.(This is the most refined grid employed in our study). It can be verified that the differences between successive approximations decay rapidly as the grid is refined. The convergence rate is equal to, approximately, 1.1.

The L_1 norm of the error in the prediction of the pressure is also frequently used as an indicator of numerical accuracy. It is defined as

$$E_{N_c}(t) = \frac{1}{N_c}\sum_{j=1}^{N_c} |p_j(t) - p_{\mathrm{ex}_j}(t)|, \tag{69}$$

where N_c is the number of computational cells of the domain, and p_j and p_{ex_j} are the computed and exact values of the pressure, respectively. Values of p_{ex_j} are calculated with a simulation using 200 points/$L_{1/2}$. Results of the numerical error at $t = 200$ are plotted in Fig. 19. The convergence rate is approximately 1.4, which is

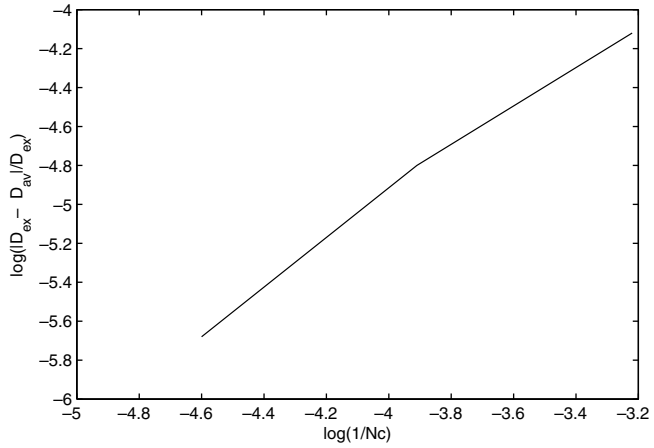

Fig. 18. Grid convergence study for case C: variation of the predicted average wave speed with the grid resolution.

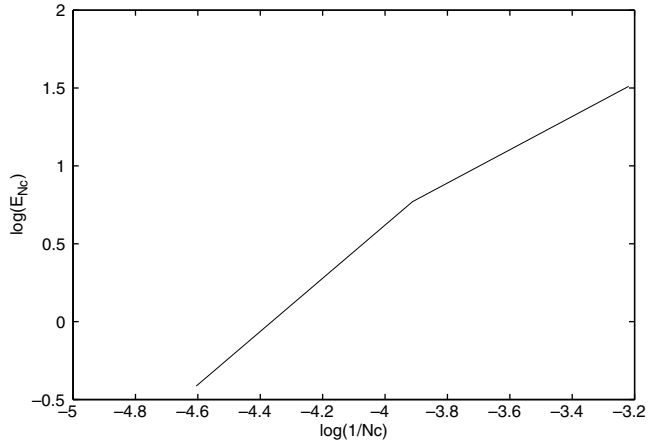

Fig. 19. Grid convergence study for case C: variation of the L_1 norm of the error in the prediction of the pressure with the grid resolution.

faster than the convergence rate of the average wave speed. In other words, the average wave speed is less sensitive to grid resolution than the pressure. This behaviour is commonly encountered in convergence studies of compressible flows in the presence of hydrodynamic discontinuities.

5.1.2. Case D: reactive particles

In this case, we consider a two-phase mixture containing reactive solid particles with $\phi_s = 5 \times 10^{-5}$. The heterogeneous reaction-parameters are $K_s = 2 \times 10^{-7}$, $q_s = 50$ and $T_{ign} = 2$. The spatial resolution of this simulation is 100 points per unit length, and it is performed with CFL = 0.5. The length of the computational domain is 2000 $L_{1/2}$.

Figs. 20–22 show profiles of pressure, gas temperature and solid volume fraction, respectively, at times $t = 40$, $t = 120$ and $t = 210$. As in the previous case, at $t = 40.0$ the detonation has not yet encountered the two-phase medium and pulsates with high pressure peaks. When the detonation reaches the contact line that separates the purely gaseous medium and the reactive heterogeneous mixture, it interacts with it and produces a transmitted detonation and a reflected inert shock. As usual, the transmitted detonation pulls the solid particles, via the momentum transfer mechanism between the two phases, leading to the formation of a compaction zone, see Fig. 22. Further, the solid particles are heated, and their temperature rapidly exceeds the

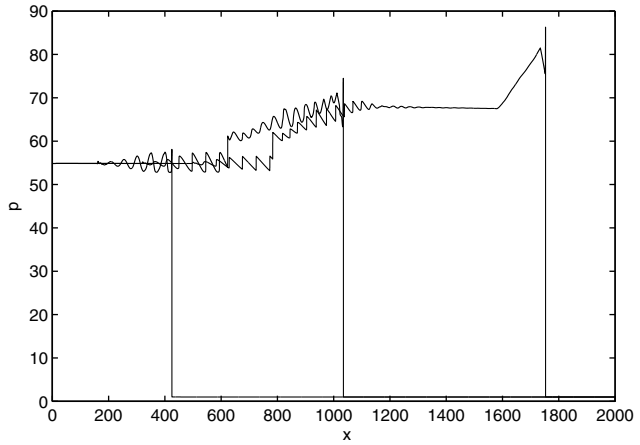

Fig. 20. Case D: pressure profiles of the transmission of a gaseous detonation to a two-phase mixture with reactive particles at times $t = 40$, $t = 120$ and $t = 210$.

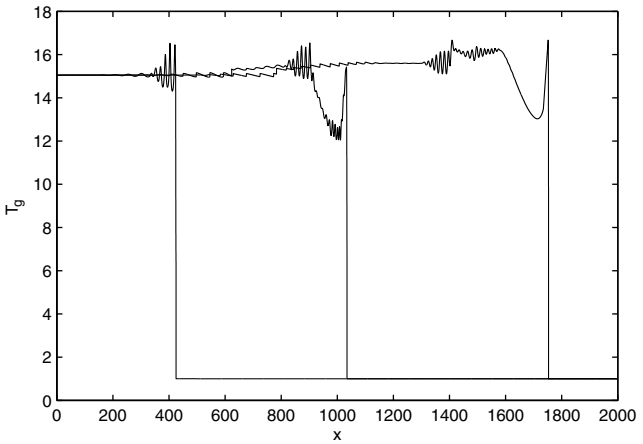

Fig. 21. Case D: gas temperature profiles of the transmission of a gaseous detonation to a two-phase mixture with reactive particles at times $t = 40$, $t = 120$ and $t = 210$.

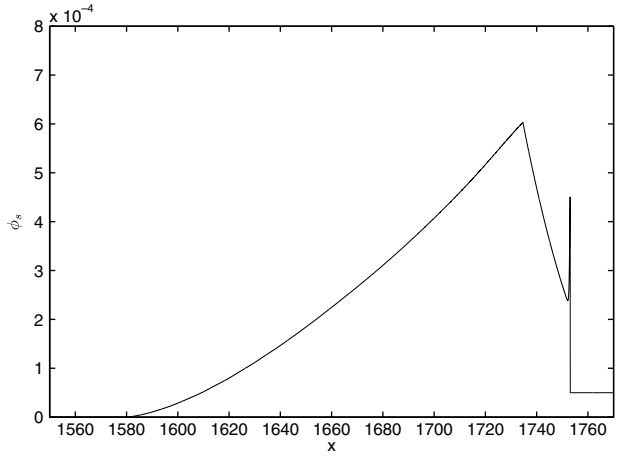

Fig. 22. Case D: solid volume fraction profile of the transmission of a gaseous detonation to a two-phase mixture with reactive particles at time $t = 210$.

threshold temperature T_{ign}, above which they begin to react. Consequently, the pressure and temperature of the resulting heterogeneous detonation behind the leading shock are considerably higher than the ones of the transmitted gaseous one.

Further, the simulation predicts that when the detonation starts propagating through the heterogeneous mixture it initially loses some of its strength and slows down but it subsequently accelerates. Its propagation velocity stabilizes at $D_{\text{av}} = 8.2$. This value is slightly higher than the minimum value predicted by (68) for the parameters of the present case ($D_{\min} = 7.68$), but still slightly lower than the propagation speed of the initial ZND detonation $D_{\text{ZND}} = 8.66$.

The detonation profile at $t = 210$ is in good agreement with the steady detonation propagating at the same speed. In particular, behind the precursor shock there is formation of the same three zones that are predicted by the steady-wave analysis in Section 4.3; see Figs. 20–22. The first one is the gaseous reaction zone inside which the pressure decreases. The second one is the induction zone, characterized by heat transfer from the gaseous phase to the solid particles and increasing pressure. Finally, the third one is the particle burning zone. It begins at the point where the solid temperature has reached the ignition value and terminates at the point where all particles are completely burnt.

5.2. Two-dimensional numerical simulation

Next, we present some preliminary results of simulations of two-dimensional heterogeneous detonations containing reactive particles. In this simulation, a steady heterogeneous detonation profile, propagating with $f = 1.6$ to the right along the x-axis, is used as initial condition. The pressure of this initial profile has been slightly perturbed along the transverse direction, in order to accelerate the growth of the flow instabilities. The dimensions of the computational domain are $40 \times 10\, L_{1/2}^2$. The spatial resolution is set at 50 points $/L_{1/2}$ and the CFL number is set at CFL $= 0.5$. The simulation is performed in the reference frame of the initial profile. Therefore, inflow conditions are imposed on the right boundary, and outflow conditions on the left boundary. On the lateral surfaces of the domain, wall boundary conditions are applied. The material specific constants are identical to those used in the 1D simulation of case B, except that in this 2D simulation we set $K_{\text{s}} = 5 \times 10^{-7}$.

Figs. 23 and 24 show contour plots for the pressure and the solid volume fraction, respectively. It can be observed that the structure of the detonation front has the typical characteristics of that of a gaseous detonation. More specifically, the flow instabilities lead to the formation of triple points that move along the shock (transversally with respect to the flow direction). Their strength and velocity are different and, therefore, they eventually collide, resulting in large over-pressures. The trajectories of the triple points form the classical cellular structure of detonations. The detonation speed is $D = 8.66$, which is close to the speed of the equivalent

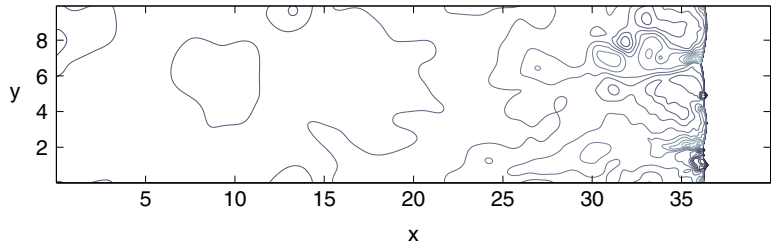

Fig. 23. Two-dimensional simulation of a heterogeneous detonation with reactive particles: pressure contours at $t = 100$.

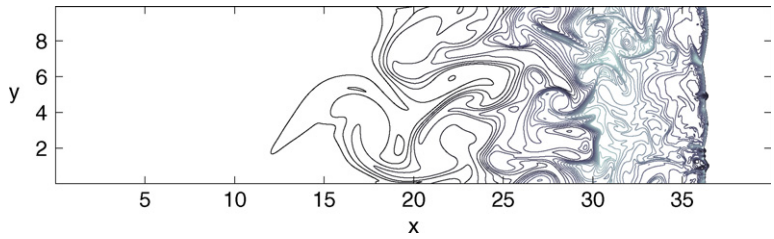

Fig. 24. Two-dimensional simulation of a heterogeneous detonation with reactive particles: ϕ_s contours at time $t = 100$.

one-dimensional steady wave. It is also interesting to mention that the flow-field behind the leading front can be sub-divided into three zones, just as in the 1D detonation that were examined earlier. In particular, we have a thin gaseous reaction zone right behind the shock, followed by the induction zone in which the burnt gas heats up the solid particles. The third zone is the heterogeneous reaction zone and it starts from the points where T_g has reached the ignition temperature and terminates at the points where the solid particles have been burnt completely, $\phi_s = 0$. As expected, this zone is longer than the other two, because the particles burn much slower than the gas.

Finally, it is worth mentioning that we have tried to compare our numerical results with experimental ones. However, there are very few experimental studies of heterogeneous detonations at low solid volume fractions. Comparisons between our numerical predictions and the available experimental data (Sedov et al. [24], Veyssière et al. [25] and Carvel et al. [26] for example) show that the proposed reduced model seems capable of accurately reproducing at least the important structures of the flow, such as secondary pressure waves and compaction zone, etc. However, a detailed quantitative comparison can not be made at this point because of three-dimensional effects and because of the simplified reaction model for the solid particles that we employ.

6. Conclusions

In this paper, we have presented and analyzed a conservative approximation to compressible two-phase flow models in the stiff mechanical relaxation limit (one-pressure one-velocity models), [15]. Such approximation can be employed when the density and sound speed of the solid phase are considerably higher than those of the gaseous phase, which is often the case in gas–solid particles mixtures of technological and industrial interest. The mixture sound speed based on the proposed conservative model is very close to the one based on [15] at low and moderate concentrations of the dispersed phase. Thus, we expect that at such concentration levels the conservative model can be used instead of its non-conservative counterpart.

A characteristic analysis reveals that the governing equations constitute a hyperbolic system of conservation laws which is complete but possesses a fivefold linear degeneracy. The Rankine–Hugoniot relations and Riemann invariants of the homogeneous part have also been derived. Further, the eigenvalue ordering is such as that the solution of the Riemann problem has the same wave ordering as the one of the classical gasdynamic Riemann problem, i.e., two waves that can be either shocks or rarefactions and a contact line between them. In the case where both phases obey a stiffened gas equation of state, the Rankine–Hugoniot

and Riemann invariants relations can be integrated analytically. These analytical expressions were employed in the development of an exact Riemann solver.

Further, the profiles of steady heterogeneous detonations have been studied. It turns out that under certain circumstances, a minimum speed of propagation exists. At the limit of very dilute mixtures this minimum speed tends to the Chapman–Jouguet velocity of gaseous detonations. The structure of the two-phase steady waves in mixtures of reactive particles is characterized by the existence of three main zones: gaseous reaction zone, induction zone (heating of the particles by the gas), and particle burning zone. On the other hand, if the particles are inert, there are only two zones: gaseous reaction zone and particle compaction zone.

These structures were also predicted numerically in the 1D and 2D simulations we performed. These simulations further showed that the presence of the particles tends to attenuate the instabilities that are inherent in gaseous detonations but also results in lower detonation speeds (with respect to gaseous detonations). Finally, our simulations predicted 2D heterogeneous detonations are also characterized by the development of triple-points along the front which eventually collide, thus forming the well-known cellular structure.

Acknowledgment

M.V.P. acknowledges with gratitude the impact and profound influence that his teacher, Professor Anthony Leonard of Caltech, exerted on the author's scientific education and research activities.

The numerical simulations presented herein were performed on the parallel computers of the Institut de Calcul Intensif et de Stockage de Masse, at UCL.

References

[1] D.A. Drew, S.L. Passman, Theory of Multicomponent Fluids, Springer, New York, 1998.
[2] H. Enwald, E. Peirano, A.E. Almstedt, Eulerian two-phase flow theory applied to fluidization, Int. J. Mult. Fluids 22 (1996) 21–66.
[3] M.R. Baer, J.W. Nunziato, A two-phase mixture theory for the deflagration-to-detonation transition in reactive granular materials, Int. J. Mult. Fluids 12 (1986) 861–889.
[4] J.B. Bdzil, R. Menikoff, S.F. Son, A.K. Kapila, D.S. Stewart, Two-phase modeling of deflagration-to-detonation transition in granular materials: a critical examination of modeling issues, Phys. Fluids 11 (1999) 378–402.
[5] J.M. Powers, D.S. Stewart, H. Krier, Theory of two-phase detonation – Part II: structure, Combust. Flame 80 (1990) 280–303.
[6] R. Saurel, R. Abgrall, A multiphase Godunov method for compressible multifluid and multiphase flows, J. Comput. Phys. 150 (1999) 425–467.
[7] M.V. Papalexandris, A two-phase model for compressible granular flows based on the theory of irreversible processes, J. Fluid Mech. 517 (2004) 103–112.
[8] K.A. Gonthier, J.M. Powers, A high-resolution numerical method for a two-phase model of deflagration-to-detonation transition, J. Comput. Phys. 163 (2000) 376–433.
[9] M.V. Papalexandris, Numerical simulations of detonations in mixtures of gases and solid particles, J. Fluid Mech. 507 (2004) 95–142.
[10] M.V. Papalexandris, Influence of inert particles on the propagation of multidimensional detonation waves, Combust. Flame 141 (2005) 216–228.
[11] N. Andrianov, G. Warnecke, The Riemann problem for the Baer–Nunziato two-phase flow model, J. Comput. Phys. 195 (2004) 434–464.
[12] V. Deledicque, M.V. Papalexandris, An exact Riemann solver for compressible two-phase flow models containing non-conservative products, J. Comput. Phys. 222 (2007) 217–245.
[13] J.M. Powers, Two-phase viscous modeling of granular materials, Phys. Fluids 16 (2004) 2975–2990.
[14] A.W. Vreman, Macroscopic theory of multicomponent flows: irreversibility and well-posed equations, Physica D 225 (2007) 94–111.
[15] A.K. Kapila, R. Menikoff, J.B. Bdzil, S.F. Son, D.S. Stewart, Two-phase modeling of deflagration-to-detonation transition in granular materials: Reduced equations, Phys. Fluids 13 (2001) 3002–3024.
[16] R. Saurel, O. Le Metayer, J. Massoni, S. Gavrilyuk, Shock jump relations for multiphase mixtures with stiff mechanical relaxation, Shock Waves 16 (2007) 209–232.
[17] J.G. Knudsen, D.L. Katz, Fluid Mechanics and Heat Transfer, McGraw-Hill, 1955.
[18] S. Chapman, T.G. Cowling, The mathematical theory of non-uniform gases, Cambridge University Press, 1961.
[19] G. Dal Maso, P.G. Lefloch, F. Murat, Definition and weak stability of nonconservative products, J. Math. Pure. Appl. 74 (1995) 483–548.
[20] P. Colella, H.M. Glaz, Efficient solution algorithms for the Riemann problem for real gases, J. Comput. Phys. 59 (1985) 264–289.
[21] K.K. Kuo, Principles of Combustion, John Wiley & Sons, New Jersey, 2005.
[22] M.V. Papalexandris, A. Leonard, P.E. Dimotakis, Unsplit schemes for hyperbolic conservation laws with source terms in one space dimension, J. Comput. Phys. 134 (1997) 31–61.

[23] M.V. Papalexandris, A. Leonard, P.E. Dimotakis, Unsplit algorithms for multidimensional systems of hyperbolic conservation laws with source terms, Comput. Math. Appl. 44 (2002) 25–49.
[24] L.I. Sedov, V.P. Korobeinikov, K.N. Shamshev, V.N. Kulikov, A.M. Lapidus, V.V. Markov, G.G. Tivanov, Effect of inert particles on the development of detonation, Sov. Phys. Doklady 35 (1990) 1021.
[25] B. Veyssière, R. Bourainnes, N. Manson, Detonation characteristics of two ethylene–oxygen–nitrogen mixtures containing aluminium particles in suspension, Gasdynamics of detonations and explosions: AIAA Prog. Astronaut. Aeronaut. 75 (1981) 423–438.
[26] R.O. Carvel, G.O. Thomas, C.J. Brown, Some observations of detonation propagation through a gas containing dust particles in suspension, Shock Waves 13 (2003) 83–89.